Copy
RM E55F01

NACA

RESEARCH MEMORANDUM

EXPERIMENTAL INVESTIGATION OF A TRANSONIC AXIAL-FLOW-COMPRESSOR ROTOR WITH DOUBLE-CIRCULAR-ARC AIRFOIL BLADE SECTIONS

III - COMPARISON OF BLADE-ELEMENT PERFORMANCE WITH THREE LEVELS OF SOLIDITY

By Francis C. Schwenk and George W. Lewis, Jr.

Lewis Flight Propulsion Laboratory
Cleveland, Ohio

NATIONAL ADVISORY COMMITTEE
FOR AERONAUTICS

WASHINGTON

July 25, 1955

NACA RM E55F01

NATIONAL ADVISORY COMMITTEE FOR AERONAUTICS

RESEARCH MEMORANDUM

EXPERIMENTAL INVESTIGATION OF A TRANSONIC AXIAL-FLOW-COMPRESSOR ROTOR WITH DOUBLE-CIRCULAR-ARC AIRFOIL BLADE SECTIONS

III - COMPARISON OF BLADE-ELEMENT PERFORMANCE WITH THREE LEVELS OF SOLIDITY

By Francis C. Schwenk and George W. Lewis, Jr.

SUMMARY

Two low-solidity transonic axial-flow-compressor rotors were tested over a range of speeds up to a corrected tip speed of 1000 feet per second to determine the performance of such rotors and to provide experimental rotor blade-element data for low solidity levels. The two rotors were 16- and 12-blade versions of a 19-blade rotor previously tested and reported. Tip solidities of the 19-, 16-, and 12-blade rotors are 1.0, 0.84, and 0.63, respectively. The rotor blade sections are double-circular-arc airfoils.

Comparisons of the hub and mean blade-element losses for the three rotors showed that the losses tended to decrease with a decrease in solidity. Hub- and mean-section losses were low for all three rotors, and measured diffusion factors were below the limiting value. Losses near the rotor tip were about the same level for the three solidities at 60 and 80 percent of design speed but increased significantly with a decrease in solidity at 90 and 100 percent of design speed.

Hub- and mean-section deviation angles for minimum-loss incidence angles were nearly constant over the speed range tested for all three rotors, and the general level of the measured deviation angles agreed with values computed from Carter's rule. However, no distinct variation of deviation angle with solidity was observed. Near the rotor tip, the deviation angles at design speed increased with decreasing solidity at a greater rate than is anticipated from Carter's rule.

Stall characteristics appeared to change with solidity, as indicated by studies made with hot-wire anemometers at 60-percent design speed. Periodic rotating stalls were observed in tests of the 19-blade rotor. However, only nonperiodic flow fluctuations were sensed in the tests of the 16- and 12-blade rotors.

INTRODUCTION

The results of testing transonic axial-flow-compressor rotors (refs. 1 to 6) have shown that compressor rotors can operate efficiently with tip-region relative inlet Mach numbers greater than 1.0. The high Mach number levels permit the design of rotors that produce high stage total-pressure ratios and pass large weight flows. These features are necessary for the design of light-weight multistage compressors for aircraft turbojet engines.

Design information for transonic compressors is, as yet, incomplete. For example, most of the reported test data deal with rotors having tip solidities (chord-spacing ratios) around 1.0 and greater (refs. 1 and 3 to 5). Some data have been reported for rotors with tip solidities around 0.75 (refs. 2 and 6). However, the effects of solidity have not been systematically investigated and reported.

Information on transonic rotors having tip solidities less than 1.0 is particularly desirable, since there are reasons that may dictate the use of low solidities. Among these reasons are blade mounting and hub choking problems that could prevent the design of a high-tip-solidity compressor rotor if the hub-tip radius ratio is low. Therefore, three related transonic rotors were tested at the NACA Lewis laboratory to investigate solidity effects at solidity levels below 1.0.

These tests were conducted on an available set of transonic rotor blades with double-circular-arc cross sections. References 5 and 7 describe these blades and present the design and over-all and blade-element performance of a 19-blade transonic rotor (tip solidity of 1.0). For the study of solidity effects, these blades were tested in 16- and 12-blade rotors that provide tip solidities of 0.84 and 0.63. At the hub, the solidities are 1.67, 1.41, and 1.05 for the 19-, 16-, and 12-blade rotors, respectively. Blade setting angles (angles of the blade mounting slots in the rotor disk) were identical for all three rotors; and, therefore, the mean camber line directions are identical. In such an investigation the velocity diagrams change with solidity, because deviation angles tend to increase with decreasing solidity. Because of these changes in the velocity diagrams, the effect of solidity will not be completely isolated. The results, however, can be used to predict solidity effects and, at the same time, to supplement existing transonic-rotor data.

The characteristics of all three rotors were determined by means of detailed radial survey tests. Complete blade-element and over-all performance characteristics of the 16- and 12-blade rotors are given in this report. References 5 and 7 give similar results for the 19-blade rotor. In addition, the present report utilizes some of the 19-blade-rotor data of references 5 and 7 for direct comparisons of the blade-element and over-all performance charactersitics for the three solidity levels.

SYMBOLS

The following symbols are used in this report:

A_F compressor frontal area based on rotor tip diameter, sq ft

c_p specific heat of air at constant pressure, Btu/(lb)(^oR)

D diffusion factor (ref. 8)

g acceleration due to gravity, 32.17 ft/sec^2

H total enthalpy, $c_p gJT$, sq ft/sec^2

i incidence angle, angle between inlet relative air-velocity vector and a tangent to blade mean camber line at leading edge, deg

J Joule's constant, 778.26 ft-lb/Btu

M Mach number

P total pressure, lb/sq ft

r radius measured from axis of rotation, in.

T total temperature, ^oR

U blade speed, ft/sec

V air velocity, ft/sec

w air weight flow, lb/sec

β air-flow angle measured from axis of rotation, deg

γ^o blade angle, direction of tangent to blade mean camber line at leading or trailing edge measured from axis of rotation, deg

δ ratio of inlet total pressure to NACA standard sea-level total pressure of 2116.22 lb/sq ft

δ^o deviation angle, angle between outlet relative air-velocity vector and tangent to blade mean camber line at trailing edge, deg

η adiabatic temperature-rise efficiency

θ ratio of inlet total temperature to NACA standard sea-level temperature of 518.688^o R

σ solidity, ratio of blade chord measured along streamline to average blade spacing

$\bar{\omega}$ relative total-pressure-loss coefficient

Subscripts:

b blade surface

m mean radius

t tip of rotor

z axial direction

1 depression tank

2 upstream of rotor, location of inlet static-pressure rake

3 rotor inlet

4 rotor-outlet survey station

Superscript:

' denotes conditions relative to blade row

APPARATUS AND PROCEDURE

The solidity tests were conducted on 16- and 12-blade versions of the 19-blade transonic compressor rotor described in references 5 and 7. The double-circular-arc blades of the 19-blade rotor were installed in two new rotor disks at the same blade setting angles. Therefore, the blade angles (given in table I) are similar for all three rotors.

References 5 and 7 describe the compressor test rig in which the rotors were tested. These references also discuss the instruments, test procedure, and calculations. Figure 1 is a diagram of the compressor test section showing the location of the measuring planes upstream and downstream of the rotor.

The rotors were tested over a range of weight flows at four corrected rotor speeds: 60, 80, 90, and 100 percent of design speed (design corrected tip speed is 1000 ft/sec).

[redacted]

DATA ANALYSIS ASSUMPTIONS

The rotor performance is analyzed by means of the blade-element approach described in reference 1. In this method, the complex compressor flow field is replaced by the flow across a series of blade elements. In applying the blade-element approach, the following assumptions are made:

(1) The state of the air is axially symmetric upstream and downstream of the compressor blade row.

(2) The flow is divided into two regions, the boundary layer near the inner and outer walls and the free-stream region outside the wall boundary layer.

(3) In the free-stream portion the flow is assumed to occur along conical stream surfaces of revolution, and the action of the blade row is the sum of the performances of the blade sections or elements that lie on the stream surfaces.

(4) The flow across each blade element is considered a function only of the section geometry, the incidence angle, the ratio of outlet to inlet axial velocities, and inlet relative Mach number. The action of the rotor can then be replaced by a radial distribution of turning angle and losses (characteristics of the blade elements).

(5) The stream surfaces were assumed the same for the three rotors discussed in this report; therefore, except for solidity, the blade-element geometry is the same for all three rotors.

The last assumption may give a fictitious picture of solidity effects on rotor blade-element performance, since it says that the flow always follows the same paths through the rotor regardless of solidity and operating condition. The successful application of this assumption depends on the radial flow of air through the rotor, which may vary with solidity level and operating condition. The use of similar blade elements for the three rotors seems justified, because, at flow rates corresponding to efficient operation at each speed, the measured radial distributions of weight flow at the rotor-inlet and -outlet stations change only slightly with changes in solidity.

BLADE-ELEMENT PERFORMANCE OF 16- AND 12-BLADE ROTORS

The blade-element characteristics for the two low-solidity (16- and 12-blade) rotors are shown in figures 2 and 3 for four blade elements and corrected rotor tip speeds of 60, 80, 90, and 100 percent of design. The four blade elements are located at 12.7, 17.7, 49.0, and 84.4 percent of the passage height away from the outer wall. The blade-element characteristics for the high-solidity rotor (19 blades) are reported in reference 7.

The characteristics shown in figures 2 and 3 are the variations with incidence angle of relative total-pressure-loss coefficient $\bar{\omega}$, deviation angle δ°, inlet relative Mach number M_3', axial velocity ratio $V_{z,4}/V_{z,3}$, diffusion factor D (ref. 8), work coefficient $\Delta H/U_t^2$ (nondimensional temperature rise), and blade-element adiabatic temperature-rise efficiency η. Incidence angles were computed from the measured blade angles and the relative inlet-air angles, which were determined according to the procedure outlined in reference 7. The large number of variables given provide complete information on the performance of these rotors and allow the construction of the velocity diagrams.

The blade-element characteristics of the 16- and 12-blade rotors are very similar to those of the 19-blade rotor (ref. 7) and other transonic-rotor data (refs. 1, 2, and 4). Therefore, the results in figures 2 and 3 will not be discussed in detail, and the data are largely used for solidity comparisons in this report.

For both the 16- and 12-blade rotors (figs. 2 and 3), the variations of relative total-pressure-loss coefficient with incidence angle and speed are similar to previously reported compressor test results (e.g., refs. 1, 2, 4, and 7). Except for the hub section of the 16-blade rotor (fig. 2(d)), there is the usual shift in the value of minimum-loss incidence angle to high values as the Mach number (speed) is increased. At the hub and mean sections (figs. 2(c) and (d) and 3(c) and (d)), the minimum losses are low and do not vary with rotational speeds. As observed in references 1, 2, 4, and 7, there is an increase in the minimum-loss level with speed associated with the sections near the rotor tip (figs. 2(a) and (b) and 3(a) and (b)). These results also show that the losses for the tip section at design speed are greater for the lower solidity. More is said about this observation in a later section.

COMPARISON OF BLADE-ELEMENT PERFORMANCE FOR THREE SOLIDITY LEVELS

Blade-Element Losses

The effects of solidity on blade-element losses are discussed in two sections. Hub and mean losses are considered first, because the performance of these elements generally compares with cascade results, and then losses at the tip elements are considered.

Hub and mean sections. - The losses for the hub and mean blade elements of the 19-, 16-, and 12-blade rotors are given in figures 4(a) and (b), where relative total-pressure-loss coefficient $\bar{\omega}$ is plotted against incidence angle. Data are shown for 60, 80, 90, and 100 percent of design corrected tip speed. The hub section is located at 15.6 percent of the passage height from the inner wall. Generally, very little effect

of solidity on losses is noticed for the range of conditions tested. Incidence-angle range seems to be the same for all solidities, and values of minimum-loss incidence angle change only slightly in the range of solidities tested.

Losses at the hub element (fig. 4(a)) increase with an increase in solidity. The loss-level change is most pronounced at design speed and is not as well defined at the lower speeds. An increase in loss level at the mean blade section with an increase in solidity can be seen in figure 4(b), although not as clearly as for the hub section. Low-speed two-dimensional cascade data (ref. 9) also show an increase in loss level with increasing solidity, as indicated by the analysis of cascade data given in reference 8.

Since the flow field probably follows two-dimensional cascade flow and the secondary-flow effects are probably small, the measured losses for the hub (15.6 percent away from the inner wall) and mean sections are primarily centered in the blade wakes. Therefore, the losses as shown in figures 4(a) and (b) depend on the size and shape of the wake leaving each blade and the number of blades present.

In order to rate the losses on a per-blade basis, the measured losses for each rotor were reduced to a loss-solidity ratio, $\bar{\omega}/\sigma$. The variation of the loss-solidity ratio with incidence angle (for hub and mean sections) is shown in figures 5(a) and (b) for 80 and 100 percent of design speed. On a per-blade basis, the losses for each solidity are about the same in the minimum-loss range of operation. To the extent of experimental accuracy, this is an indication that the size and shape of the blade wake are much the same for the three rotor solidities. In retrospect, little effect of solidity on the loss per blade should have been observed in these tests for two reasons: (1) The solidity at the hub and mean was not reduced enough to cause excessive blade loading and flow separation to occur, and (2) below limiting loading, the variation of loss-solidity ratio with loading is small and probably within measurement accuracy.

The first reason is illustrated in figures 6(a) and (b). These figures present the loss-solidity ratio plotted against diffusion factor (blade-loading parameter, ref. 8) for the hub and mean sections. Only data near minimum-loss operation are given in figure 6, since the diffusion factor applies only in the low-loss range of incidence angle. Reference 8 states a value of 0.6 for limiting loading (diffusion factor) for cascades, and figure 6 shows that for all solidities the measured diffusion factors were less than 0.6 for the hub and mean sections. Figure 6 shows no appreciable change in loss-solidity ratio with diffusion factor below limiting loading.

Tip section. - The losses for the tip blade elements of the 19-, 16-, and 12-blade rotors are given in figure 4(c). The blade-element is located at 12.7 percent of the passage height from the outer wall, and data are given for 60, 80, 90, and 100 percent of design speed. The value for

the minimum-loss incidence angle decreases slightly with decreasing solidity. At high speeds, the change in the minimum-loss incidence angle is about 1° to $1\frac{1}{2}^\circ$ over the range of solidities tested.

One fact stands out on these curves. At the low speeds, the minimum-loss level is nearly the same for each solidity; whereas, at 90 and 100 percent of design speed, the minimum-loss level increases with the decrease in solidity. This trend is most noticeable at design speed and is opposite that of the hub and mean sections. The test results indicate that the increase in loss level with a decrease in solidity occurs only in the tip region. That is, this reversal in solidity effect was not observed for a blade element located 33 percent of the passage height away from the outer wall. Instead, for this 33-percent blade element, the loss variation with solidity was similar to the trends observed at the hub and mean elements and from cascade data.

These tests results introduce the following questions:

(1) Why do tip-section losses increase with decreasing solidity in opposition to the trends observed at the hub and mean?

(2) Why does this reversed solidity effect appear only at high speeds?

As an attempt to answer these questions, it is first desirable to look at some of the conventional flow parameters on which losses may depend and to determine their variation with solidity in these tests. Among the conventional flow parameters are inlet relative Mach number and blade loading as expressed by diffusion factor D (ref. 8). It is also suspected that axial velocity ratio (outlet to inlet) may also affect the loss level.

Inlet relative Mach number, of course, does not change with solidity in this investigation. As shown in figure 7, the measured axial velocity ratios $V_{z,4}/V_{z,3}$ do not vary with solidity; and figure 8 shows that measured diffusion factors are about the same for the three rotors.

The measured tip-section losses are compared with some previously published results in figure 9, where the relative total-pressure-loss coefficient for operation near minimum-loss incidence angle is plotted against diffusion factor D. The dashed lines in figure 9 represent the band of data observed for tip sections in reference 8. The 19-blade-rotor data fall within the band for all speeds. Up to 90 percent of design speed, the 16- and 12-blade-rotor data also correlate with earlier test results. However, at design speed, the losses for the lower-solidity rotors fall above the band, the 12-blade data being farther out of line than the 16-blade data.

Therefore, the increase in tip-section losses associated with a decrease in solidity is not accounted for by changes in diffusion factor, axial velocity ratio, and inlet Mach number levels. Solidity changes, then, must have caused differences in the tip-region flow field at design speed that cannot be measured by these gross flow parameters. Exactly what changes in the flow field occur with solidity changes is unknown; therefore, concrete reasons for the occurrence of high losses at low solidity levels in these tests cannot be given.

Some factors that could conceivably cause the increase in tip losses with a decrease in solidity are as follows:

(1) Adverse changes in blade-surface velocity distributions that may cause flow separation

(2) Changes in secondary flows in the wall and blade surface boundary layers

(3) Changes in the secondary flows of the free-stream portion of the air flow

(4) Changes in rotor tip-clearance effects.

To illustrate the manner in which an adverse suction-surface velocity distribution could arise at low solidity, consider the two-dimensional supersonic flow about a cascade of airfoils shown in a very simplified form in figure 10. This figure shows an approximate picture of the shock-wave configurations for the tip-section (r_4 = 6.62 in.) airfoils in a two-dimensional cascade at two solidity levels (1.04 and 0.66). A design-speed (supersonic inlet relative velocity) operating condition with a back pressure on the cascade is used for the comparison; thus, a detached bow wave is shown.

Blade surface Mach numbers computed by means of a two-dimensional Prandtl-Meyer expansion (assuming no losses) are also shown in figure 10. The Mach numbers indicate the relative strength of the normal shock waves at the suction surface for the two solidity levels. As shown in figure 10, conditions that cause suction-surface separation are likely to be worse for the low solidity levels, because

(a) The pressure rise across the shock wave is greater at low solidity because of the higher blade-surface Mach number, and

(b) The shock waves hit closer to the trailing edge where the boundary layer may be somewhat thicker.

The preceding discussion presents only a possible source of the high losses at low solidities, and it is based on a simplified picture of the

flow in the tip region, neglecting changes in stream-tube height through the rotor. Actually, local changes in the three-dimensional effects (items (2), (3), and (4)) could also contribute to adverse velocity distributions at low solidity levels. Changes in the tip-region flow field due largely to secondary-flow and tip-clearance effects cannot be overlooked. For example, decreasing the solidity could alter the blade scraping action near the casing so that larger losses could occur.

In general, the increase in losses with a decrease in solidity probably results from several causes, no one cause being completely independent of the others.

Deviation Angles

The variations of deviation angle with incidence angle are compared for the three rotors in figure 11. Data for the hub, mean, and tip sections at 60, 80, 90, and 100 percent of design speed are given.

The deviation angles for the minimum-loss incidence angles are plotted in figure 12 against percent of design speed for the 19-, 16-, and 12-blade rotors. The values of deviation angle plotted in figure 12 were taken from the faired curves of figure 11. The minimum-loss incidence angles were estimated from figure 4, a plot of loss coefficient against incidence angle.

Some remarks regarding the selection of rotor speeds for the abscissa of figure 12 are necessary. Rotor speed is not a fundamental independent variable; it is merely a means to catalog the data. Changes in rotor speeds imply variations in the flow characteristics, which in turn affect the deviation angles. Furthermore, even for fixed speeds, the flow characteristics will vary with solidity.

The study of measured rotor deviation angles can be simplified by comparing the results with deviation angles measured in two-dimensional cascades. Such a comparison is given in figure 12, and Carter's rule for airfoils having circular-arc mean camber lines is the source of the cascade data. Previous rotor data have shown that Carter's rule applies to the selection of design deviation angles. Carter's rule (ref. 10) is

$$\delta^{\circ} = m\Phi\sqrt{\frac{1}{\sigma}}$$

where m depends on chord angle and is a constant for one blade element, and the camber angle Φ is also fixed for a given blade element. Therefore, the deviation angles computed from Carter's rule as shown in figure 12 reflect the geometric effect of a change in solidity. For the ranges of solidity covered in these tests, the changes in deviation angle with solidity according to Carter's rule are about 1.5° at the hub and 1° at the tip.

At the hub and mean radii (figs. 12(a) and (b)), the measured rotor deviation angles at minimum-loss incidence angles are roughly the same level as the Carter's rule values; however, no distinct variations with solidity are present in the measured results. Generally, the deviation angles for the hub and mean are nearly constant over the speed range tested.

For the tip section (fig. 12(c)), the 19- and 16-blade measured deviation angles are nearly constant over the speed range tested. These data are lower than the Carter's rule value. For the tip section, the deviation angle increases with decreasing solidity, as expected from cascade results. However, at design speed the change in deviation angle with solidity is much greater than the variation observed at low speeds and from Carter's rule. The larger deviation-angle changes at design speed are caused by the increase in tip-section losses with decreasing solidity (fig. 4(c)) and indicate a possible flow separation on the blade suction surface.

RADIAL VARIATION OF ROTOR-INLET AND -OUTLET CONDITIONS AND OVER-ALL PERFORMANCE

Rotor-Inlet Conditions

Rotor-inlet conditions are presented to show the measured inlet velocity profiles used in the blade-element performance calculations. Data for the three rotors are given to indicate possible effects of changes in solidity and rotor performance on the inlet velocity profile. The rotor-inlet conditions shown in figure 13 are the radial variations of inlet absolute Mach number plotted as the ratio of Mach number to mean-radius Mach number. The figure gives the variations for 80 and 100 percent of design speed and for a range of weight flows at each speed. The inlet velocity direction was assumed as axial (no inlet guide vanes), and the radial static-pressure variation for rotor-inlet calculations was faired between outer- and inner-wall static-tap readings at station 3 (1/8 in. upstream of rotor hub). In fairing, a radial trend similar to that recorded from the inlet static rake and wall taps at station 2 (1 in. upstream from station 3) was used. This procedure seemed reasonably correct, since there were only a small area change and small static-pressure differences between stations 2 and 3.

In the analysis of the 19-blade rotor performance (ref. 7), a radial variation of inlet Mach number was observed. A similar profile existed at the high-weight-flow operating points for all speeds. At the low weight flows, changes in the inlet Mach number profile were associated with high tip losses and stalling of the blades.

The inlet Mach number profiles for all three rotors are similar at the high weight flows (fig. 13). However, at design speed (fig. 13(a)), a change in the inlet Mach number variation is observed for the 12-blade rotor at $w\sqrt{\theta}/\delta A_F$ of 27.4. For the same weight flow, the change in the profile was not observed for the 19- and 16-blade rotors. Similar trends are observed at 80 percent of design speed; the inlet Mach number variations are similar at high weight flows, and a change in the variation is noted at low-weight-flow operation of each rotor.

It is interesting to note that, at the low weight flows for which a change in the inlet Mach number profile occurred, the outer-wall static pressures at station 3 were slightly higher than outer-wall pressures at station 2.. This observation is not consistent with the decrease in area from station 2 to 3 and is opposite to the wall static-pressure variation observed at the high weight flows.

Rotor-Outlet Conditions

The radial variations of blade-element temperature-rise efficiency η, total-pressure ratio P_4/P_1, and work coefficient $\Delta H/U_t^2$ for the 19-, 16-, and 12-blade rotors are plotted in figure 14. These results are given for design and 80 percent of design speed and one corrected weight flow for each rotor. All rotors were operating close to peak efficiency for the conditions shown in figure 14. Also, nearly equal weight flows were chosen for the three rotors. These rotor-outlet conditions are shown largely to indicate the manner in which the blade-element performance should be faired to reconstruct the characteristics of the complete rotor row.

The difference in total-pressure ratio at 80 percent of design speed can be traced to changes in work coefficient with solidity (fig. 14(b)). Since the losses and work coefficient tend to decrease with decreasing solidity, the efficiencies do not vary from one rotor to the next.

At design speed, there is a large increase in the tip-region total-pressure ratio with increasing solidity (fig. 14(a)). This change stems partly from work-coefficient variations and partly from the decrease in losses with an increase in solidity. Near the tip, the loss-solidity variation causes a decrease in efficiency with a decrease in solidity. However, the efficiency near the hub is highest for the lowest solidity, because, in this region, the observed losses tended to decrease with decreasing solidity.

Over-All Performance

The mass-averaged rotor performance data are plotted in figure 15 against the corrected weight flow per unit frontal area (specific weight

flow) as computed from the orifice data. Given in the plot are the mass-averaged total-pressure ratio and the mass-averaged temperature-rise efficiency for the three rotor solidities. Data are presented for 60, 80, 90, and 100 percent of design speed for a weight-flow range at each speed.

The average total-pressure-ratio level increases with increasing solidity for all speeds similarly to the work-coefficient variation shown in figure 14. Small differences in total-pressure level are shown at low speeds and large differences at design speed. At the low speeds, where the loss levels do not vary greatly with solidity, the increase in total-pressure ratio stems largely from the increase in the work-coefficient level. However, at design speed, the large variations in tip-section losses along with the work-coefficient variation cause large increases in total-pressure level with increasing solidity.

The peak efficiencies at design speed are about the same for the 19- and 16-blade rotors. Therefore, the higher losses observed in the tip region of the 16-blade rotor must be counterbalanced by the observed lower losses near the rotor hub. The 12-blade-rotor peak-efficiency values at 90 and 100 percent of design speed are at a lower level than for the 19- and 16-blade rotors. Excessive tip losses for this rotor along with a decrease in work coefficient with decreasing solidity cause this efficiency change.

At 80 percent of design speed, the peak-efficiency values tend to increase with decreasing solidity, and the opposite trend appears at 60-percent speed. These variations of efficiency level, particularly at 60-percent speed, may not be significant, because of measurement errors.

Stall Characteristics

Hot-wire anemometers were placed downstream of the rotors to detect the stall characteristics of the 16- and 12-blade rotors at 60-percent design speed. Reference 5 describes the stall characteristics of the 19-blade rotor, which operated with periodic rotating stalls at low weight flows at 60-percent design speed. However, periodic stalls were not observed in the tests of the 16- and 12-blade rotors at the low weight flows.

The observations made with the hot-wire anemometers on the 16- and 12-blade rotors at 60-percent design speed can be summarized as follows:

(1) At high weight flows, the hot-wire anemometers detected only blade wakes.

(2) After the weight flow was reduced to a value below that for the peak pressure ratio, the blade wakes were obscured by large flow fluctuations in the tip region. These flow fluctuations can best be described

as a random or nonperiodic stall. At 60-percent design speed, the nonperiodic type of stall persisted for corrected specific weight flows as low as 10 pounds per second per square foot of frontal area. This weight flow is below the values for which rotating stalls were observed in the 19-blade rotor.

SUMMARY OF RESULTS

Two low-solidity versions of a previously reported transonic axial-flow-compressor rotor were tested to provide some data on the performance of low-solidity compressor rotors that operate at high levels of rotor-inlet relative Mach numbers (up to 1.1). The original rotor contained 19 blades and had a tip solidity of 1.0. Rotors having tip solidities of 0.84 and 0.63 were constructed by placing first 16 and then 12 of the original blades in new rotor disks. Blade-element characteristics of the 16- and 12-blade rotors were computed from detailed survey test data for a range of corrected tip speeds up to the design value of 1000 feet per second and are plotted against incidence angle in this report. The blade-element loss characteristics of the two low-solidity rotors were generally similar to previously reported rotor test results.

Comparison of the losses for the 19-, 16-, and 12-blade rotors in the hub and mean regions of the blade showed that

1. The relative total-pressure-loss coefficient tends to increase with increasing solidity; however, on a per-blade basis, the hub- and mean-section losses were about the same for all three rotors.

2. Hub- and mean-section minimum-loss levels were generally low, and blade loadings (diffusion factors) were below the limiting value.

Comparison of the blade-element losses in the tip region for the 19-, 16-, and 12-blade rotors showed that

1. At the low rotor speeds (60 and 80 percent of design speed), the minimum-loss levels near the tip were about the same for the three solidity levels.

2. At design and 90 percent of design speed, losses increased with decreasing solidity. A larger increase in loss occurred at design speed.

3. Up to 90 percent of design speed, the tip-section losses of all three rotors agreed with previous rotor test results on the basis of the loss - diffusion-factor correlation. At design speed, only the 19-blade-rotor loss data correlated with previously reported data.

[redacted]

Comparison of the measured deviation angles at minimum-loss incidence angles for the 19-, 16-, and 12-blade rotors showed that

1. The hub- and mean-section deviation angles were about constant over the speed range tested, and the general level of the measured deviation angles agreed with deviation angles computed from Carter's rule. However, no distinct variations of measured deviation angle with solidity were observed.

3530

2. Tip-section deviation angles of the 16- and 19-blade rotors were nearly constant over the speeds tested and slightly below the value computed from Carter's rule. Tip-section deviation angles at design speed increased with decreasing solidity, a greater amount than was calculated from Carter's rule.

Hot-wire-anemometer tests at 60-percent design speed showed changing stall patterns with solidity. The anemometer sensed periodic stall patterns with the 19-blade rotor and only large nonperiodic flow fluctuations at the rotor tip with the 16- and 12-blade rotors.

Lewis Flight Propulsion Laboratory
National Advisory Committee for Aeronautics
Cleveland, Ohio, June 2, 1955

REFERENCES

1. Schwenk, Francis C., Lieblein, Seymour, and Lewis, George W., Jr.: Experimental Investigation of an Axial-Flow Compressor Inlet Stage Operating at Transonic Relative Inlet Mach Numbers. III - Blade-Row Performance of Stage with Transonic Rotor and Subsonic Stator at Corrected Tip Speeds of 800 and 1000 Feet Per Second. NACA RM E53G17, 1953.

2. Robbins, William H., and Glaser, Frederick W.: Investigation of an Axial-Flow-Compressor Rotor with Circular-Arc Blades Operating up to a Rotor-Inlet Relative Mach Number of 1.22. NACA RM E53D24, 1953.

3. Tysl, Edward R., Schwenk, Francis C., and Watkins, Thomas B.: Experimental Investigation of a Transonic Compressor Rotor with a 1.5-Inch Chord Length and an Aspect Ratio of 3.0. I - Design, Over-All Performance, and Rotating-Stall Characteristics. NACA RM E54L31, 1955.

4. Montgomery, John C., and Glaser, Frederick W.: Experimental Investigation of a 0.4 Hub-Tip Diameter Ratio Axial-Flow Compressor Inlet Stage at Transonic Inlet Relative Mach Numbers. II - Stage and Blade-Element Performance. NACA RM E54I29, 1955.

[redacted]

5. Lewis, George W., Jr., Schwenk, Francis C., and Serovy, George K.: Experimental Investigation of a Transonic Axial-Flow-Compressor Rotor with Double-Circular-Arc Airfoil Blade Sections. I - Design, Over-All Performance, and Stall Characteristics. NACA RM E53L21a, 1954.

6. Savage, Melvyn, and Felix, A. Richard: Investigation of a High-Performance Axial-Flow Compressor Transonic Inlet Rotor Designed for 37.5 Pounds Per Second Per Square Foot of Frontal Area. Aerodynamic Design and Over-All Performance. NACA RM L55A05, 1955.

7. Lewis, George W., Jr., and Schwenk, Francis C.: Experimental Investigation of a Transonic Axial-Flow-Compressor Rotor with Double-Circular-Arc Airfoil Blade Sections. II - Blade-Element Performance. NACA RM E54J08, 1955.

8. Lieblein, Seymour, Schwenk, Francis C., and Broderick, Robert L.: Diffusion Factor for Estimating Losses and Limiting Blade Loadings in Axial-Flow-Compressor Blade Elements. NACA RM E53D01, 1953.

9. Herrig, L. Joseph, Emery, James C., and Erwin, John R.: Systematic Two-Dimensional Cascade Tests of NACA 65-Series Compressor Blades at Low Speeds. NACA RM L51G31, 1951.

10. Carter, A. D. S.: The Low Speed Performance of Related Airfoils in Cascade. Rep. No. R. 55, British N.G.T.E., Sept. 1949.

TABLE I. - ROTOR BLADE-ELEMENT GEOMETRY

Radius, in.		Solidity, σ			Measured blade inlet angle, γ_3^o, deg	Measured blade outlet angle, γ_4^o, deg
Inlet, r_3	Outlet, r_4	12-Blade	16-Blade	19-Blade		
7.00	7.00	0.63	0.84	1.00	52.7	41.5
6.55	6.62	.66	.88	1.04	51.0	37.2
6.38	6.47	.67	.89	1.06	50.2	35.6
5.80	5.97	.71	.95	1.13	47.6	30.0
5.22	5.47	.78	1.04	1.23	44.7	23.7
4.63	4.97	.85	1.14	1.35	41.5	16.7
4.05	4.47	.95	1.27	1.51	37.6	8.3
3.50	4.00	1.05	1.41	1.67	[a]33.5	[a]-1.0

[a]Angles are extrapolated values.

[redacted]

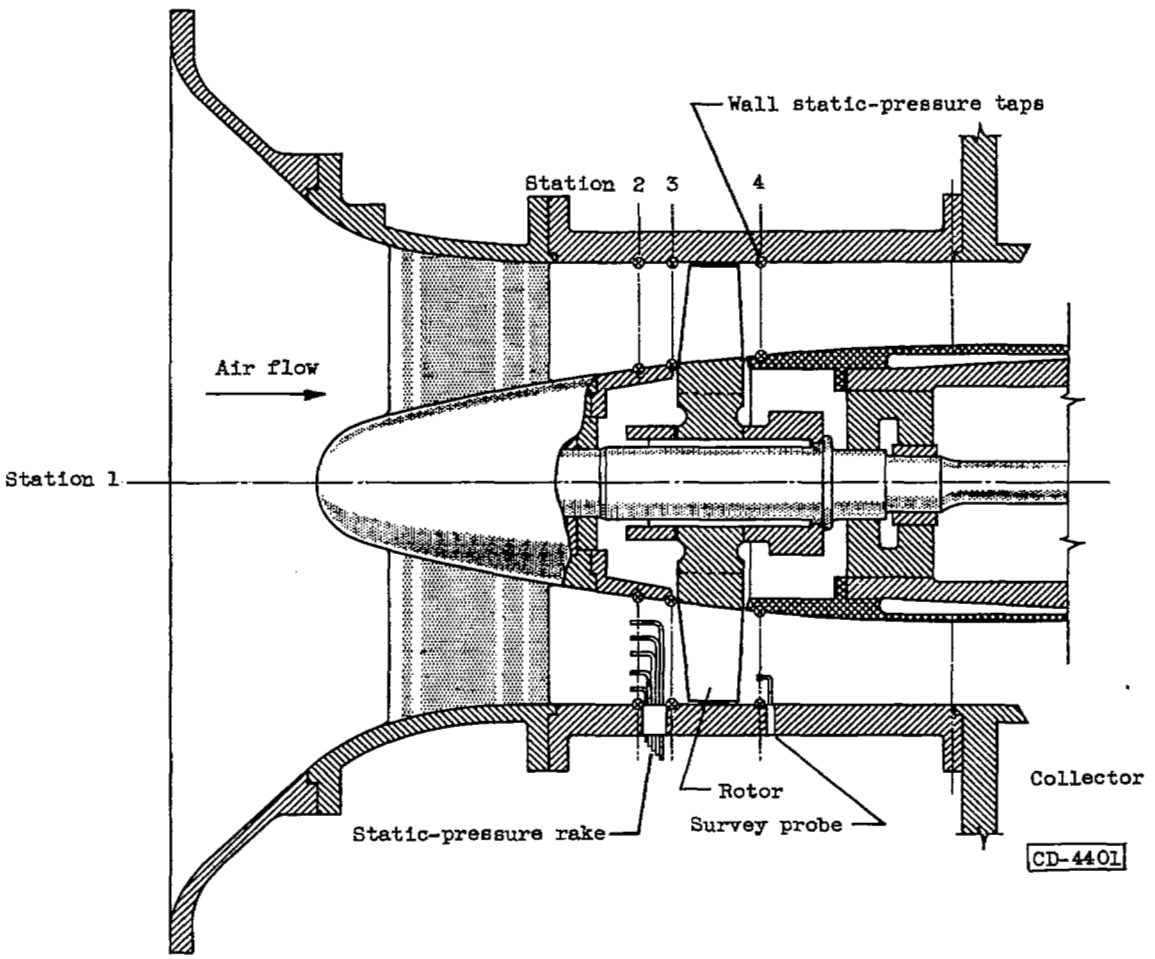

Figure 1. - Schematic diagram of transonic-compressor test rig.

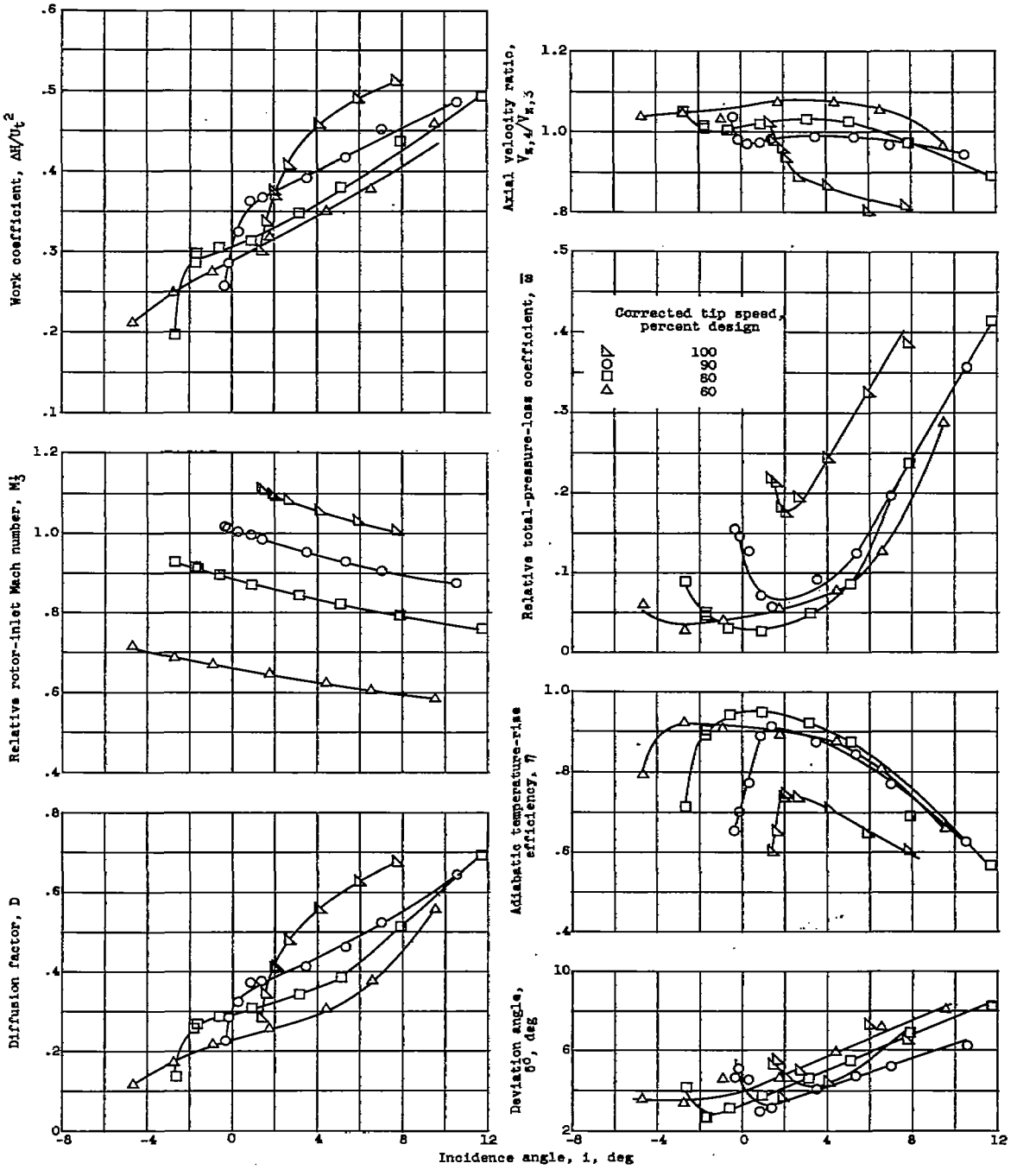

(a) Outlet radius (tip), 6.62 inches; solidity, 0.88.

Figure 2. - Blade-element characteristics of 16-blade rotor.

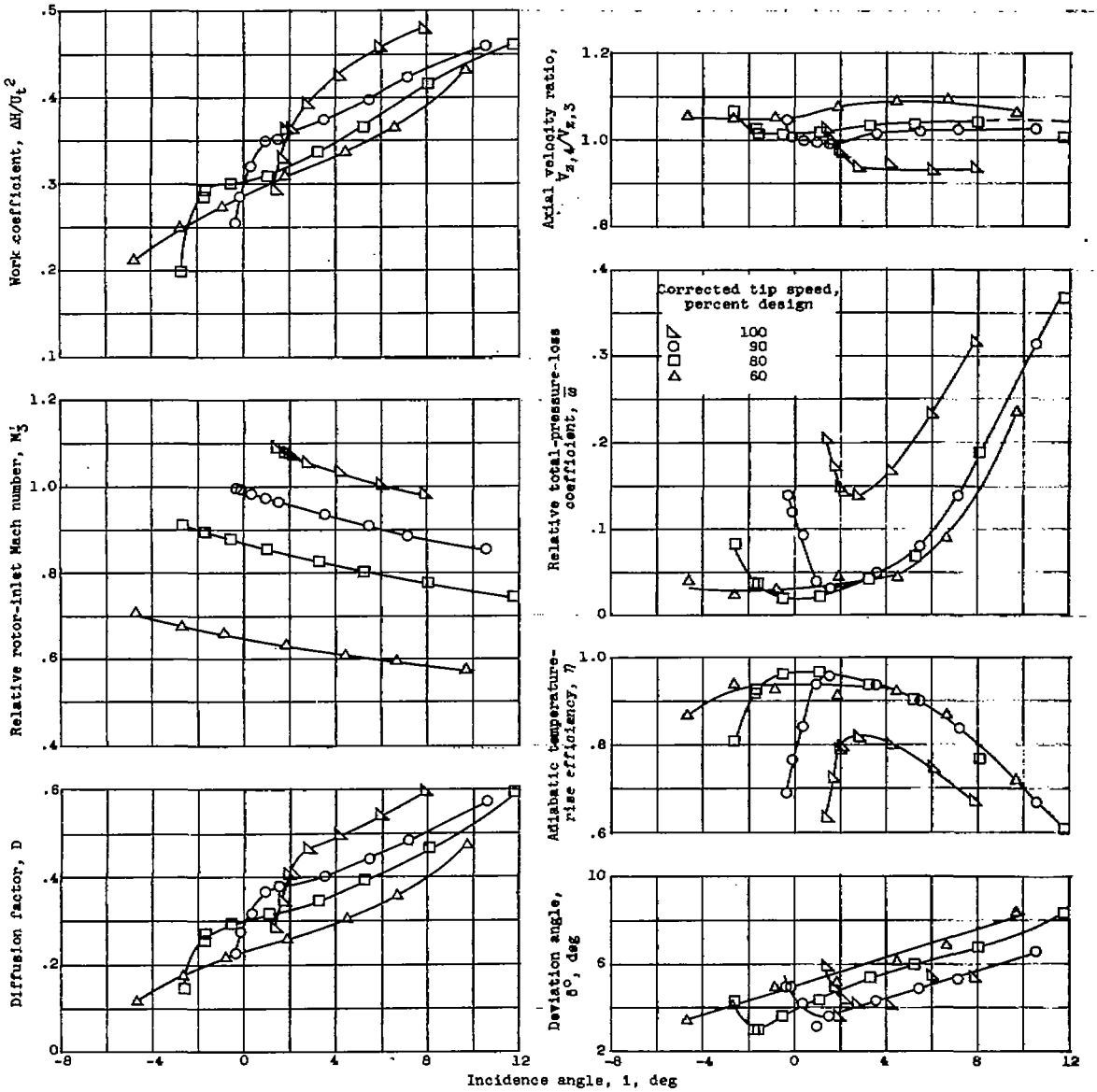

(b) Outlet radius, 6.47 inches; solidity, 0.89.

Figure 2. - Continued. Blade-element characteristics of 16-blade rotor.

[redacted]

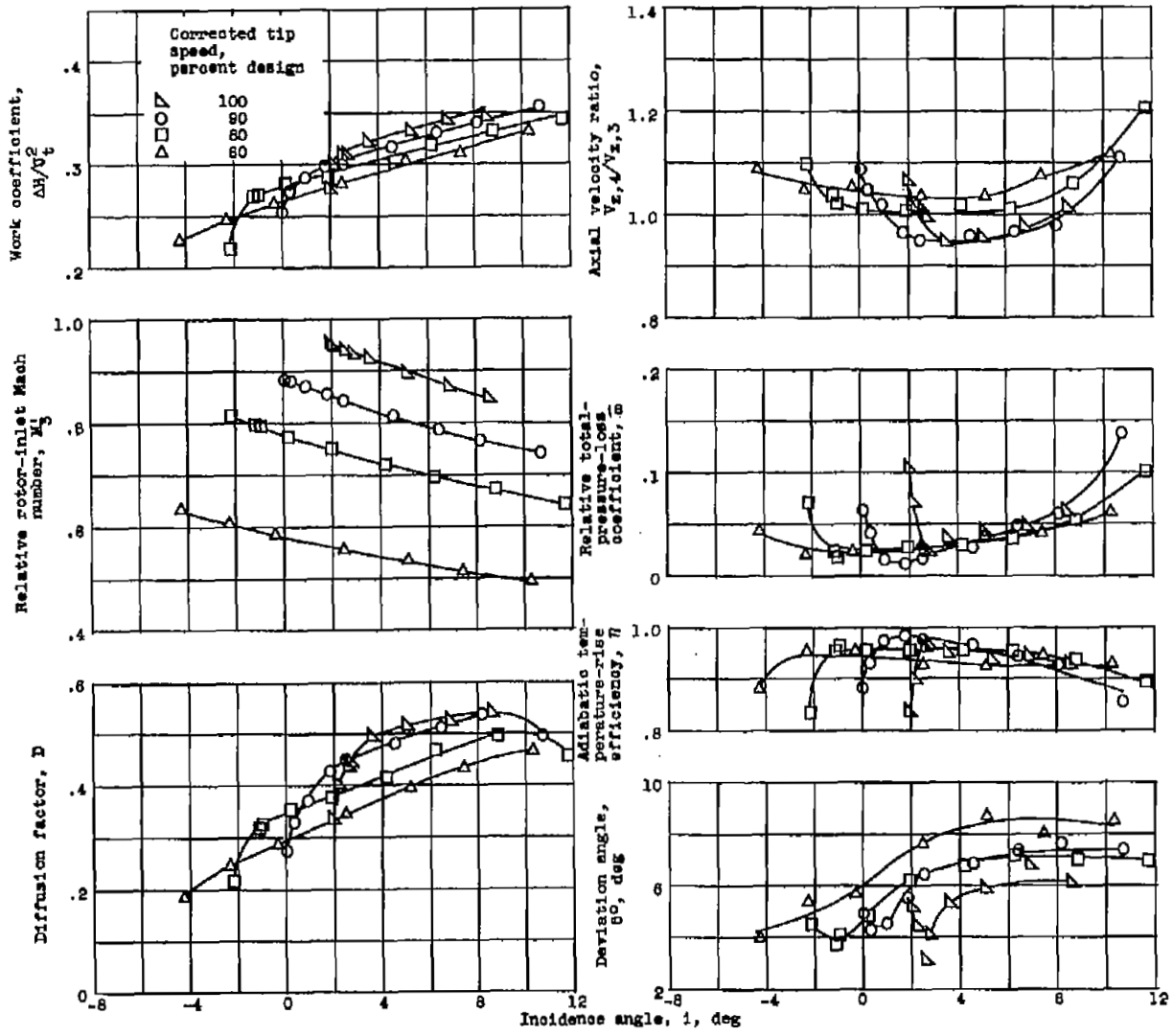

(a) Outlet radius (mean), 5.47 inches; solidity, 1.04.

Figure 2. - Continued. Blade-element characteristics of 16-blade rotor.

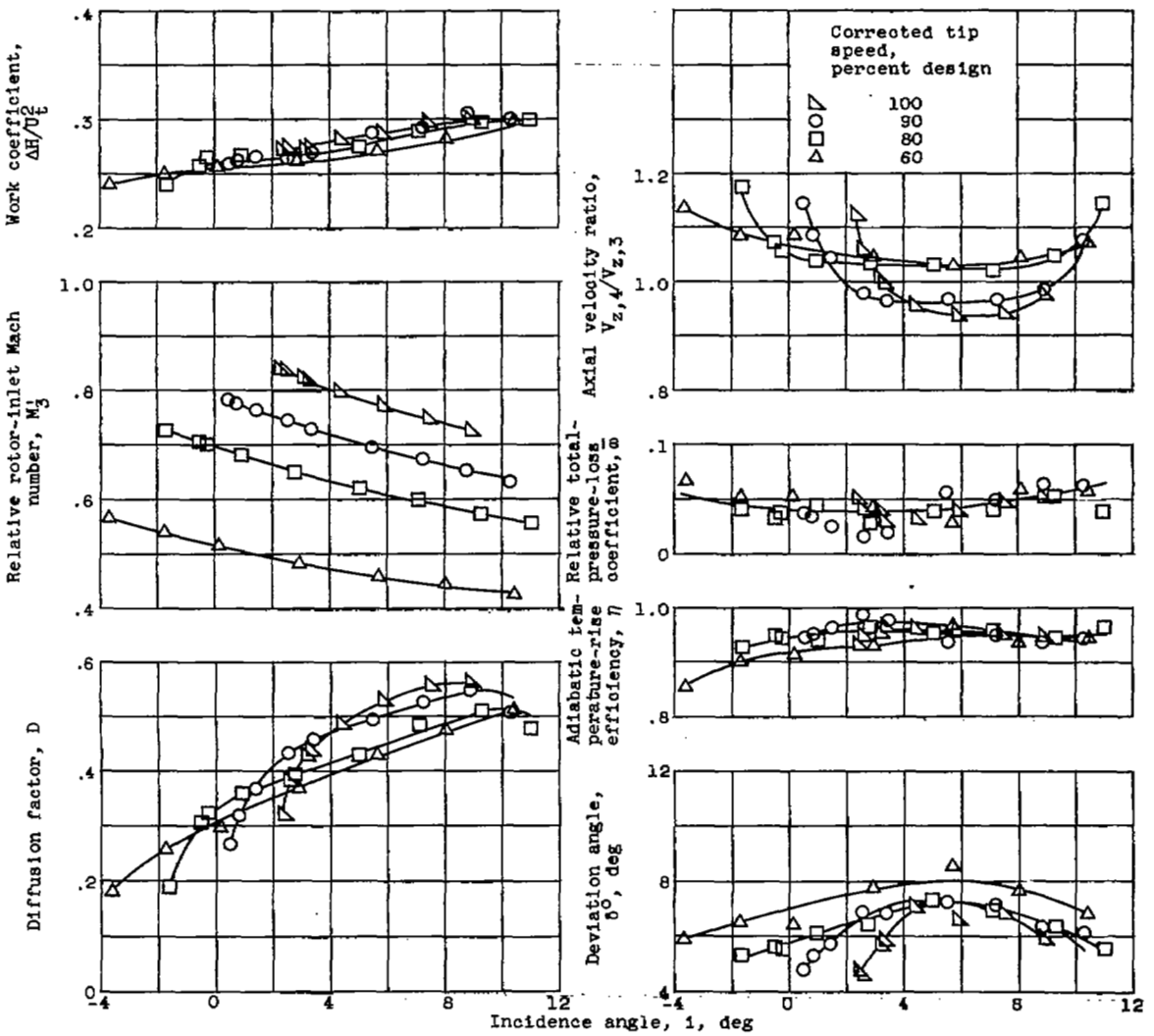

(d) Outlet radius (hub), 4.47 inches; solidity, 1.27.

Figure 2. - Concluded. Blade-element characteristics of 16-blade rotor.

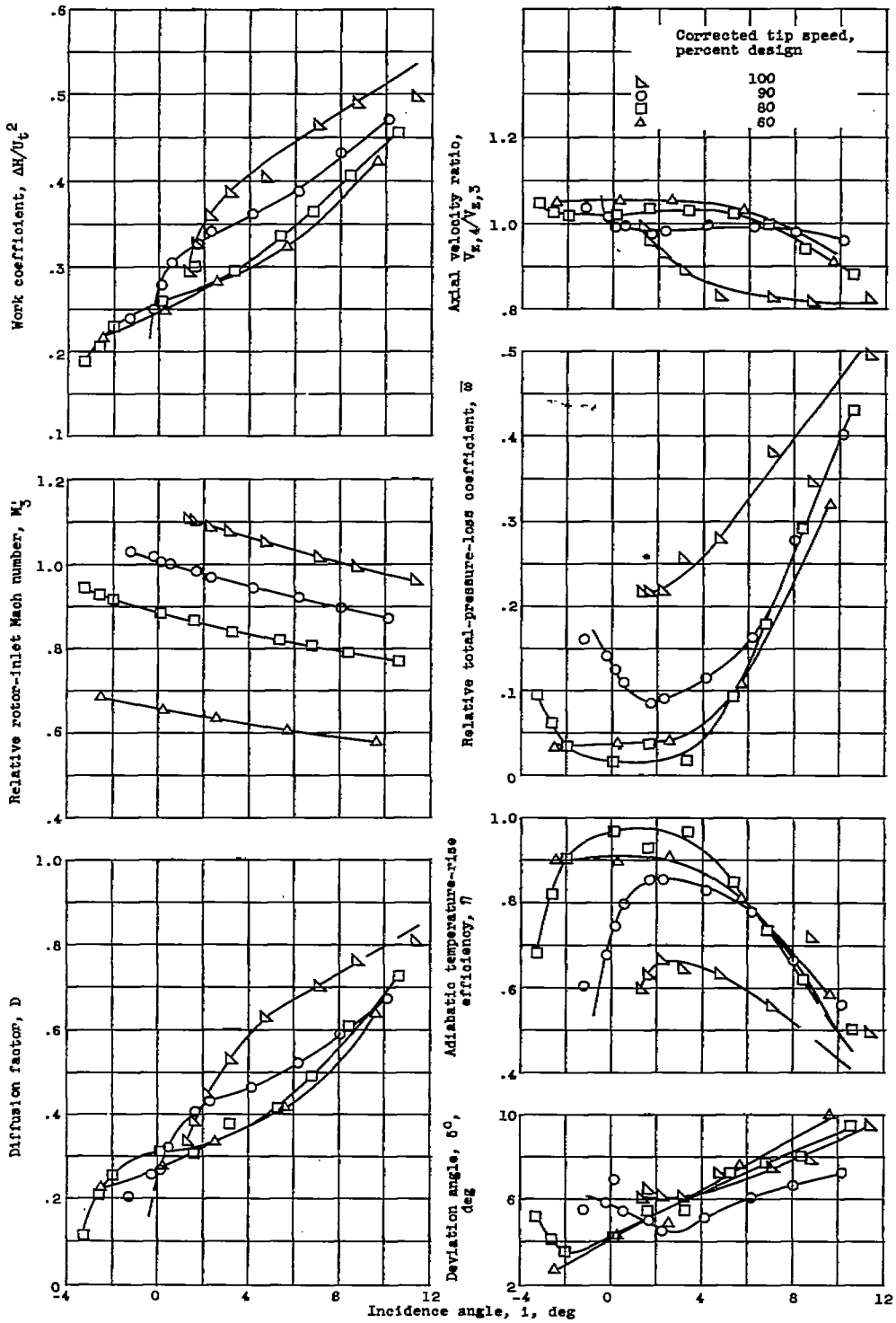

(a) Outlet radius (tip), 6.62 inches; solidity, 0.66.

Figure 3. - Blade-element characteristics of 12-blade rotor.

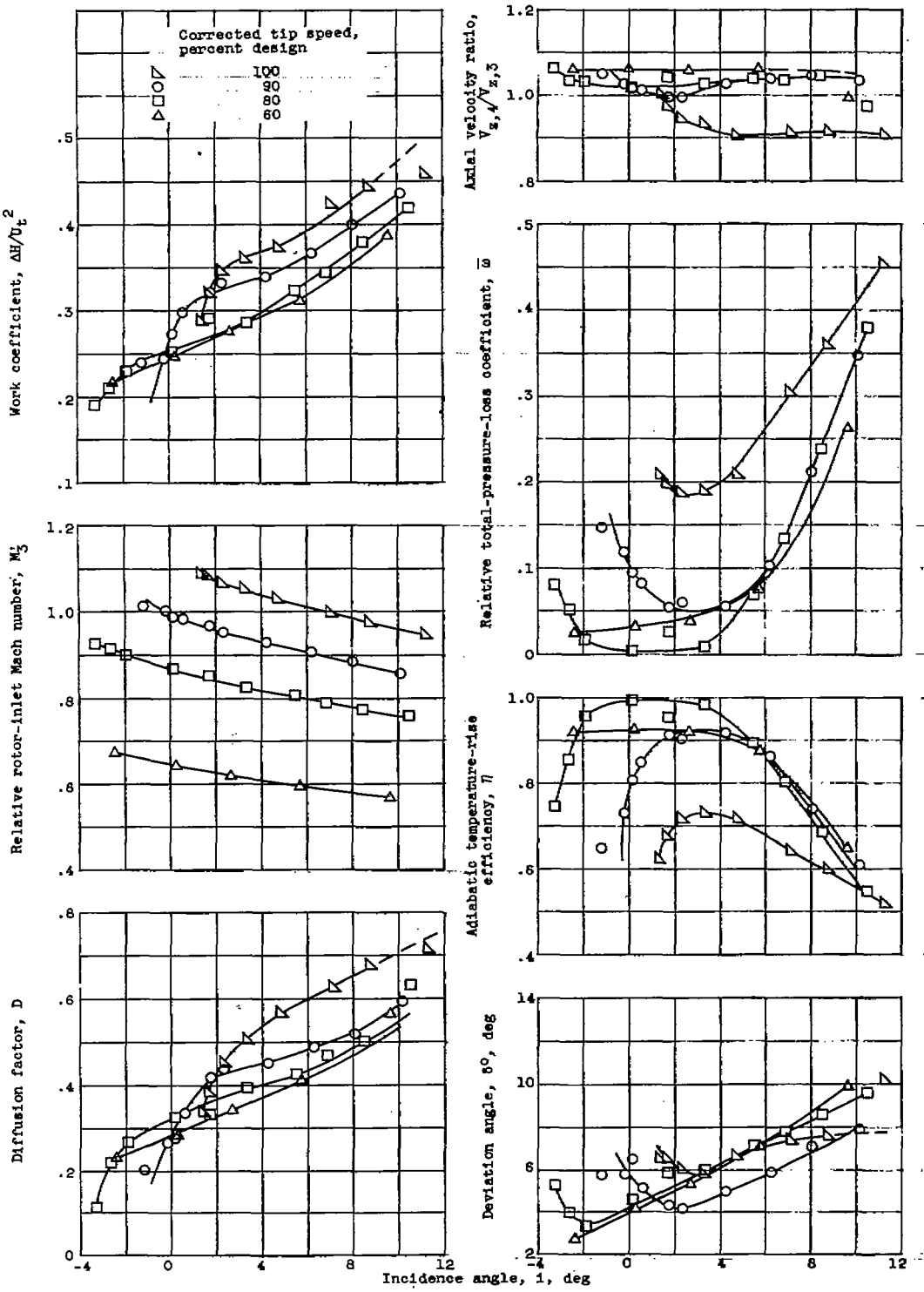

(b) Outlet radius, 6.47 inches; solidity, 0.67.

Figure 3. - Continued. Blade-element characteristics of 12-blade rotor.

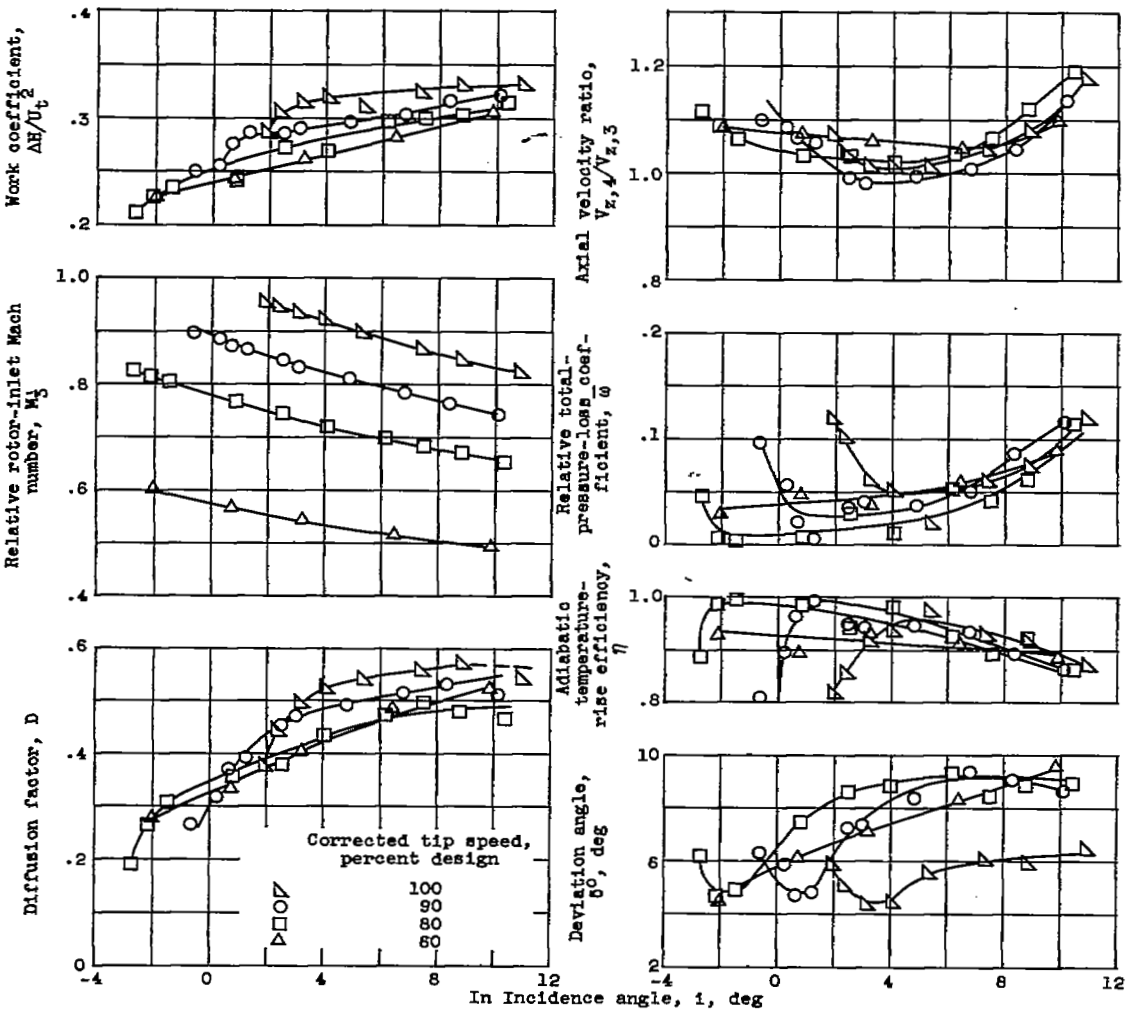

(c) Outlet radius (mean), 5.47 inches; solidity, 0.78.

Figure 3. - Continued. Blade-element characteristics of 12-blade rotor.

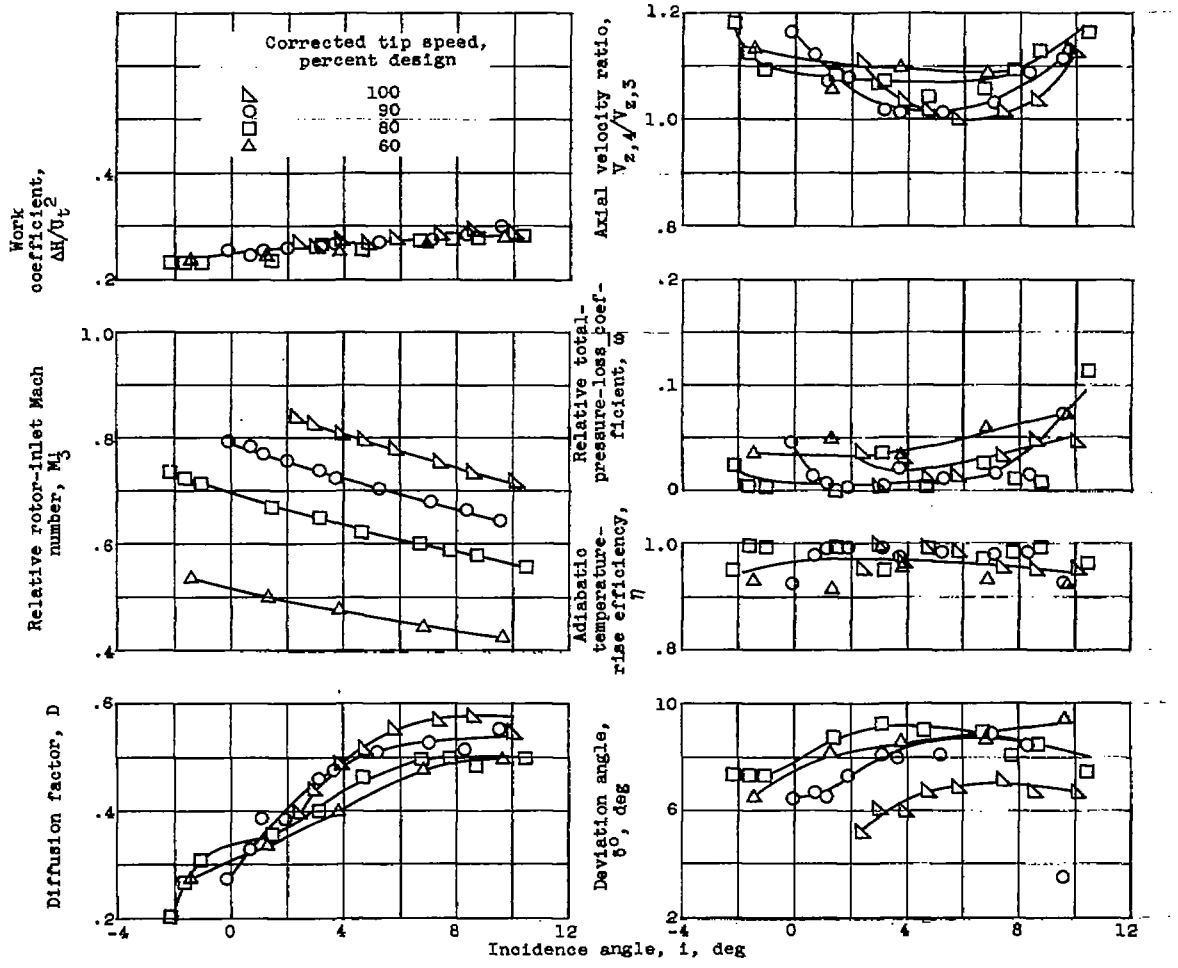

(d) Outlet radius (hub), 4.47 inches; solidity, 0.95.

Figure 3. - Concluded. Blade-element characteristics of 12-blade rotor.

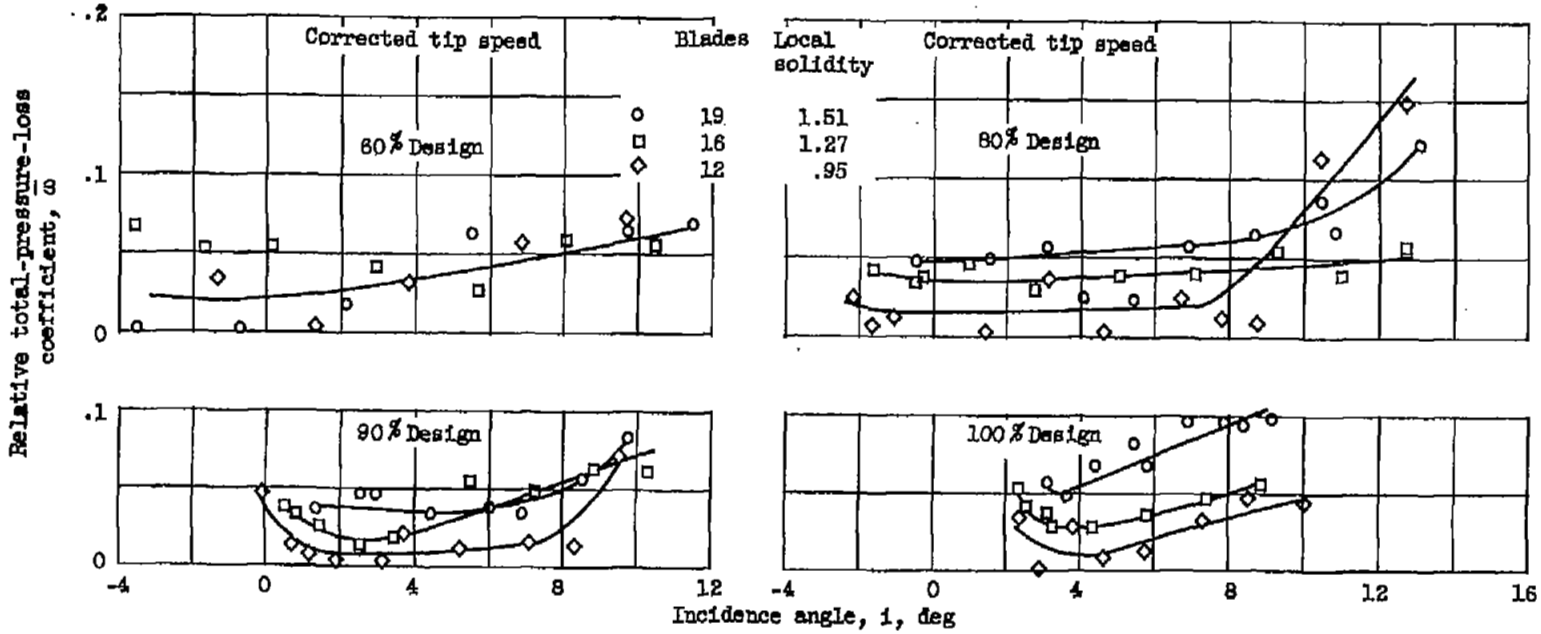

(a) Outlet radius (hub), 4.47 inches.

Figure 4. - Variation of relative total-pressure-loss coefficient with incidence angle for three solidity levels.

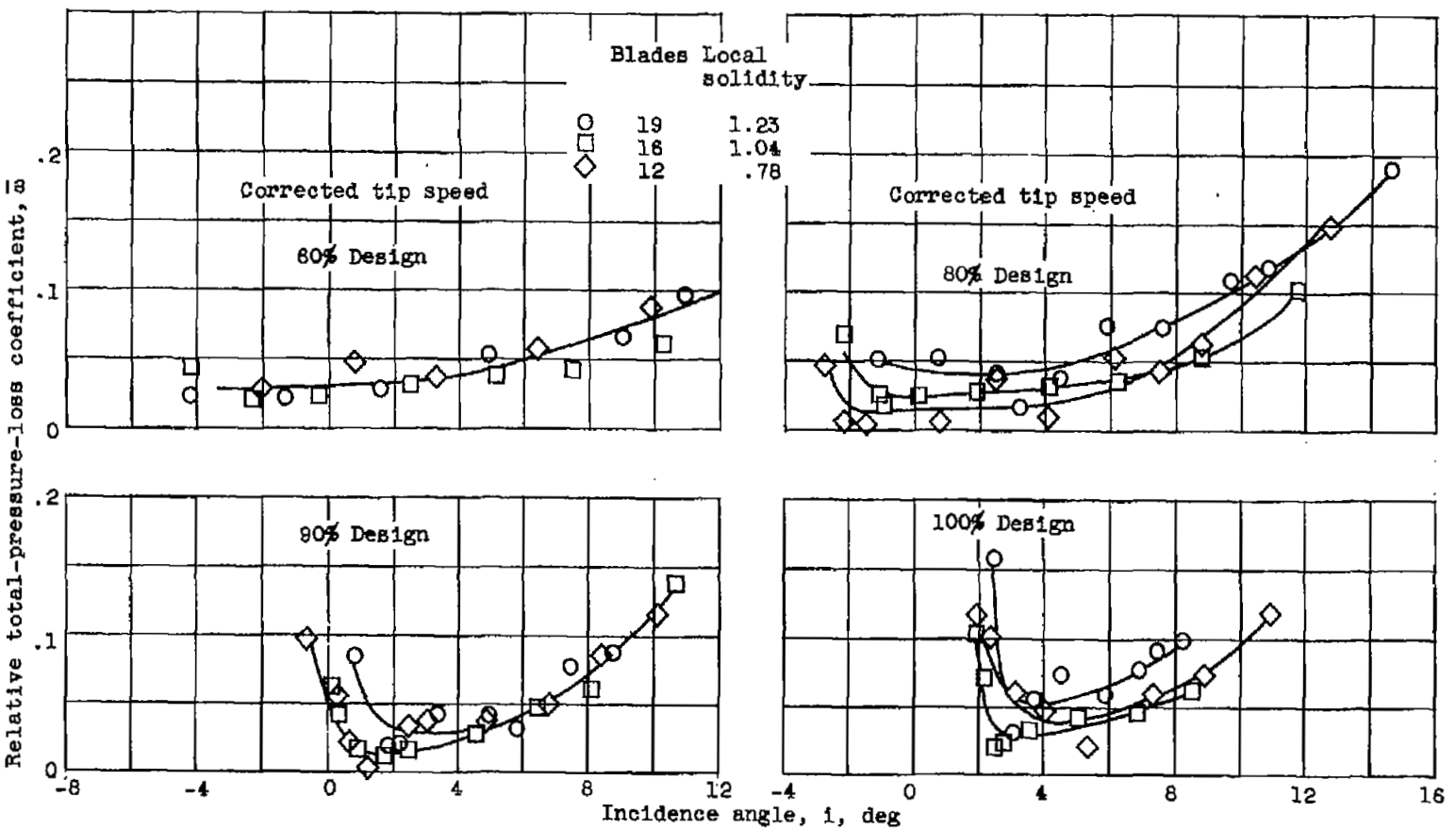

(b) Outlet radius (mean), 5.47 inches.

Figure 4. - Continued. Variation of relative total-pressure-loss coefficient with incidence angle for three solidity levels.

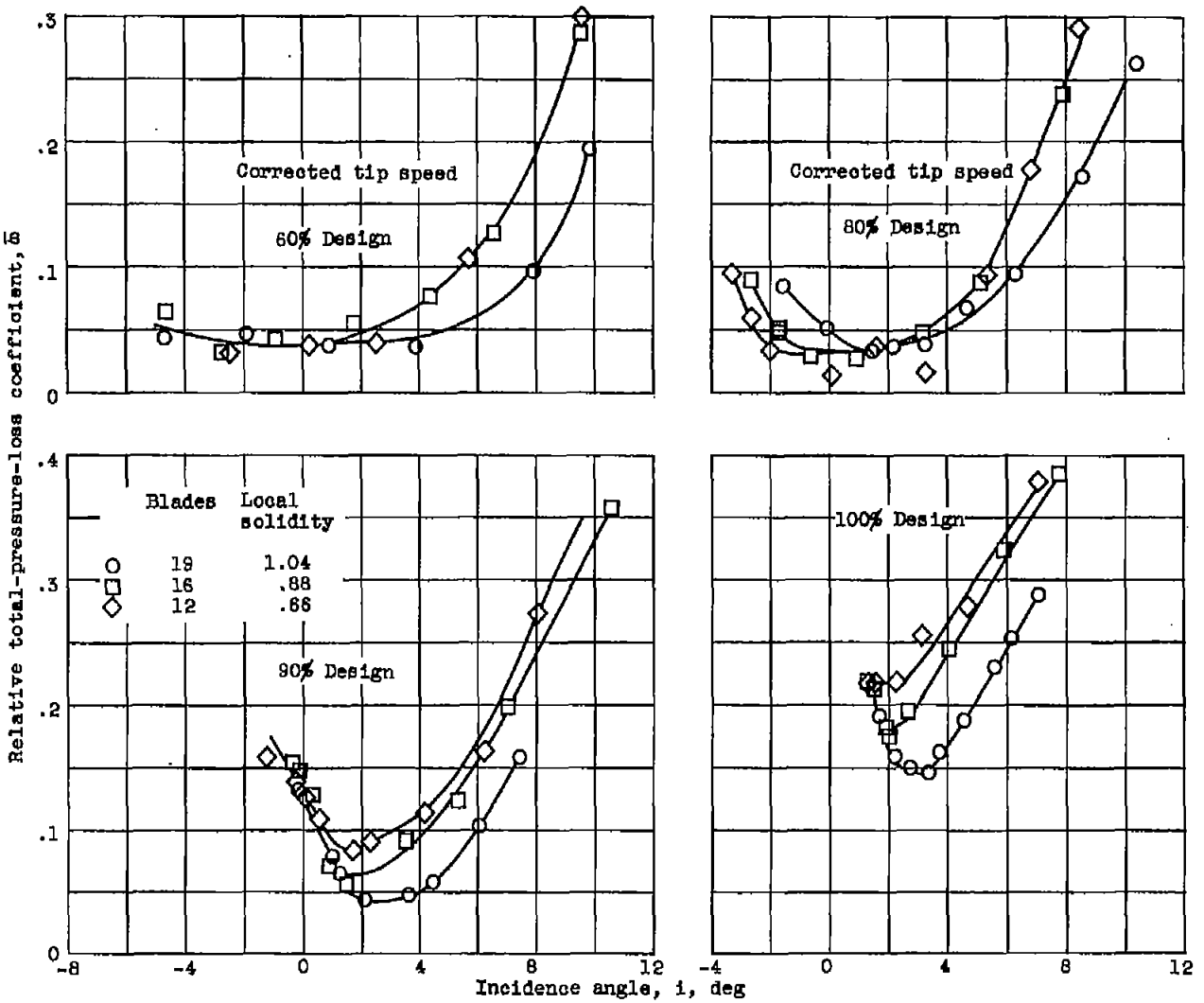

(c) Outlet radius (tip), 6.62 inches.

Figure 4. - Concluded. Variation of relative total-pressure-loss coefficient with incidence angle for three solidity levels.

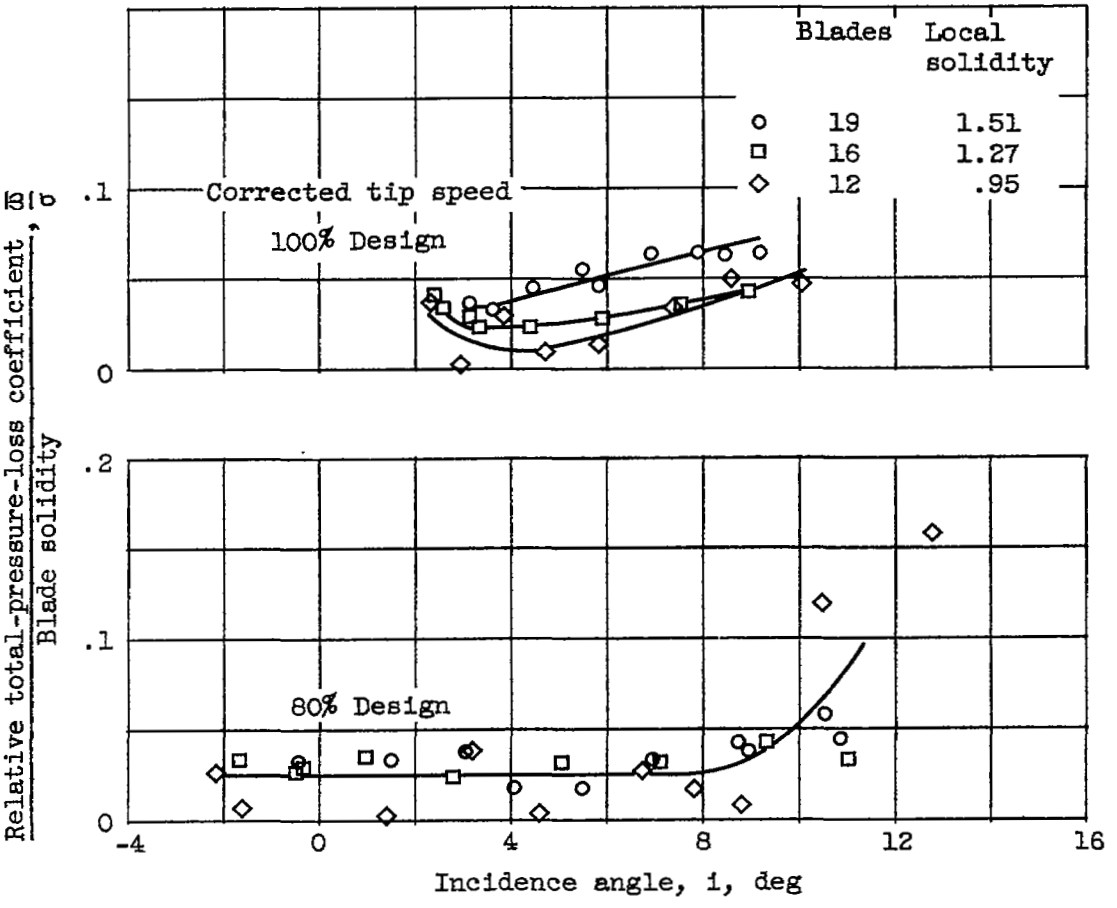

(a) Outlet radius (hub), 4.47 inches.

Figure 5. - Variation of loss-solidity ratio with incidence angle for three solidity levels.

[redacted]

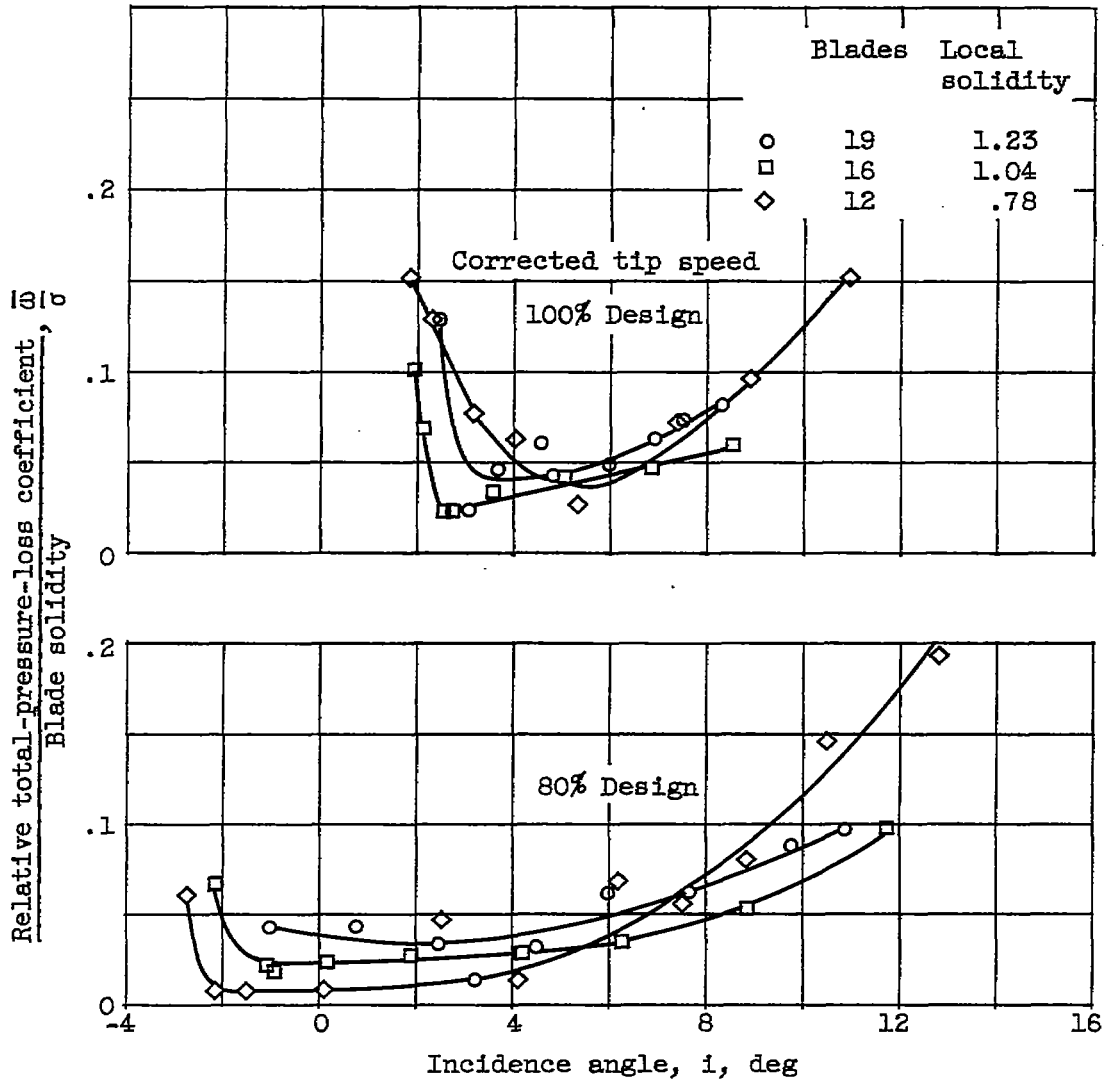

(b) Outlet radius (mean), 5.47 inches.

Figure 5. - Concluded. Variation of loss-solidity ratio with incidence angle for three solidity levels.

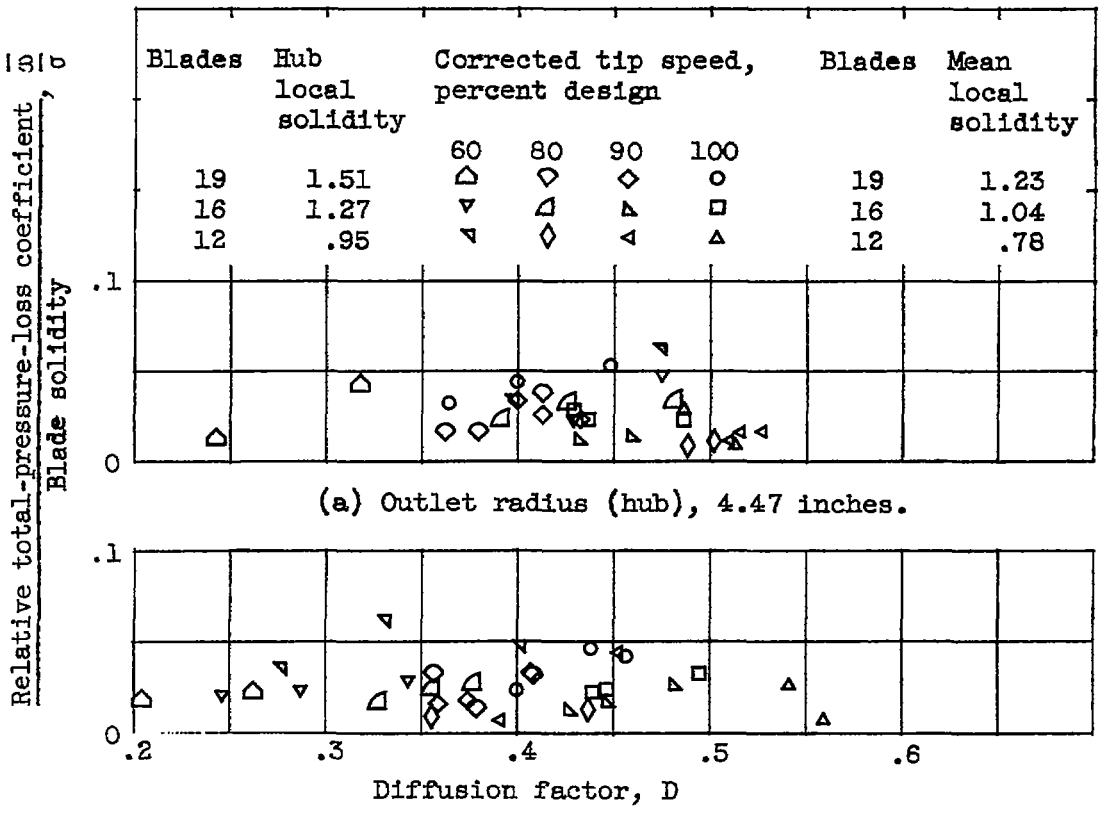

(a) Outlet radius (hub), 4.47 inches.

(b) Outlet radius (mean), 5.47 inches.

Figure 6. - Variation of loss-solidity ratio near minimum-loss incidence angle with diffusion factor for three solidity levels.

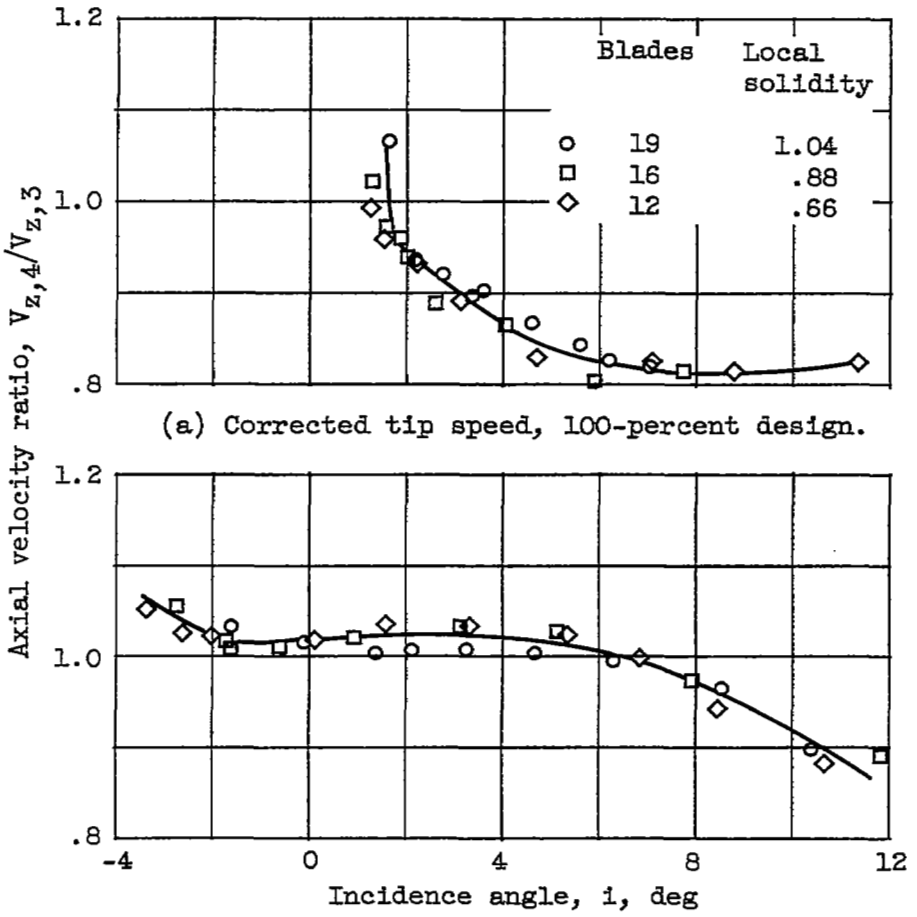

Figure 7. - Variation of tip-section axial velocity ratio with incidence angle for three solidity levels. Outlet radius, 6.62 inches.

[redacted]

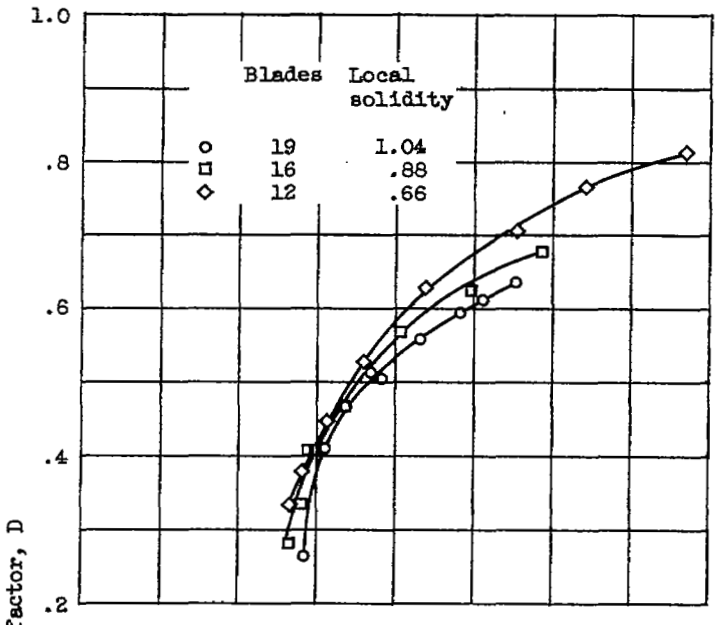

(a) Corrected tip speed, 100-percent design.

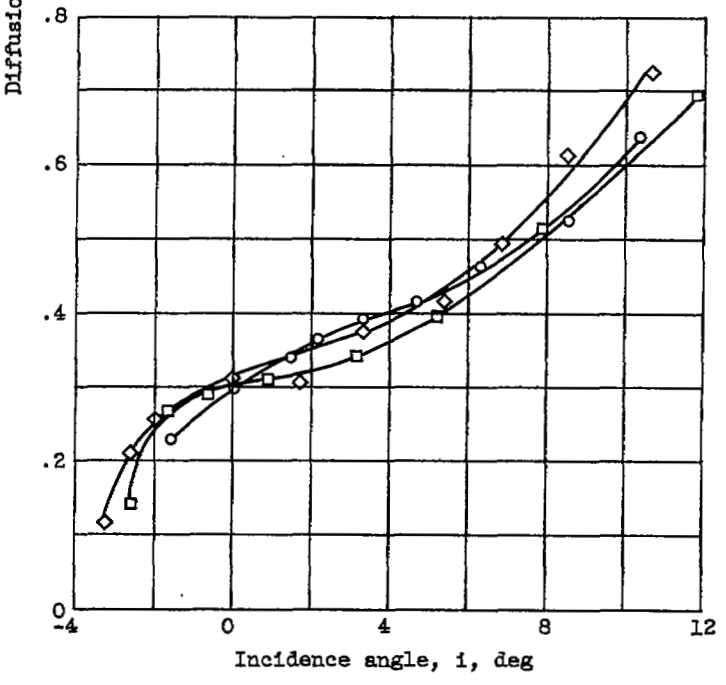

(b) Corrected tip speed, 80-percent design.

Figure 8. - Variation of tip-section diffusion factor with incidence angle for three solidity levels. Outlet radius, 6.62 inches.

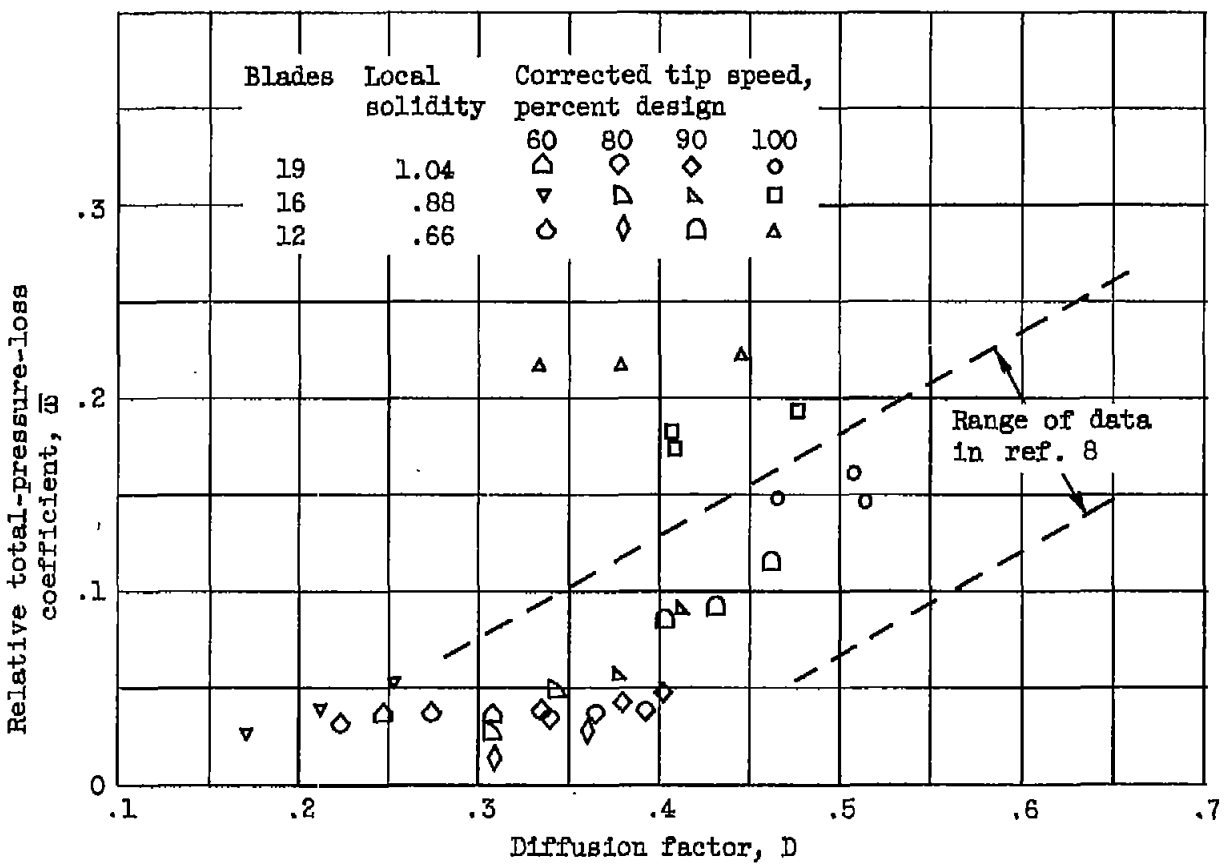

Figure 9. - Variation of relative total-pressure-loss coefficient near minimum-loss incidence angle with diffusion factor for three solidity levels. Outlet radius, 6.62 inches.

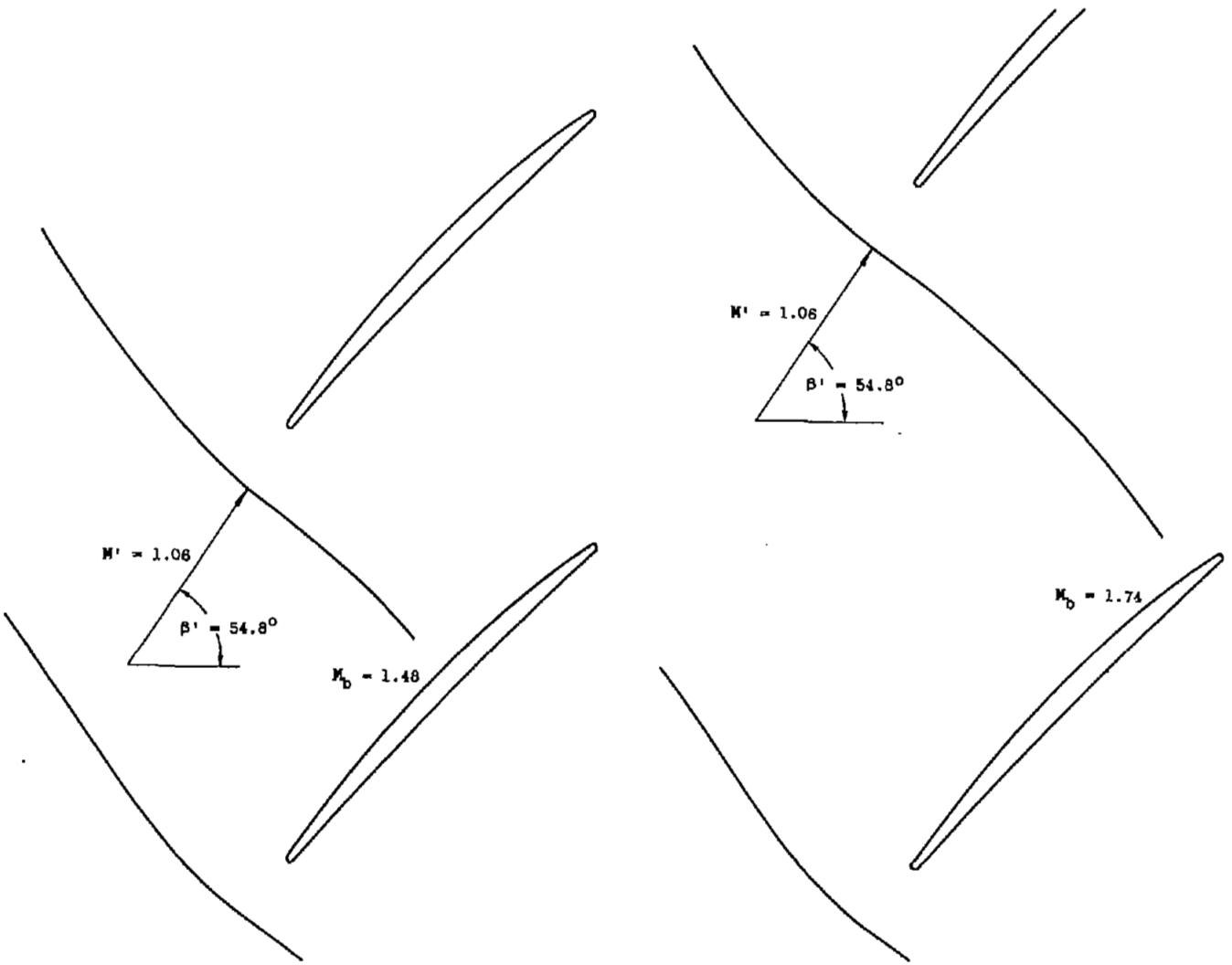

(a) 19-Blade rotor. Solidity, 1.04.

(b) 12-Blade rotor. Solidity, 0.66.

Figure 10. - Supersonic flow through a cascade indicating change in location of bow wave and resulting higher blade surface Mach numbers with decrease in solidity. Outlet radius, 6.62 inches.

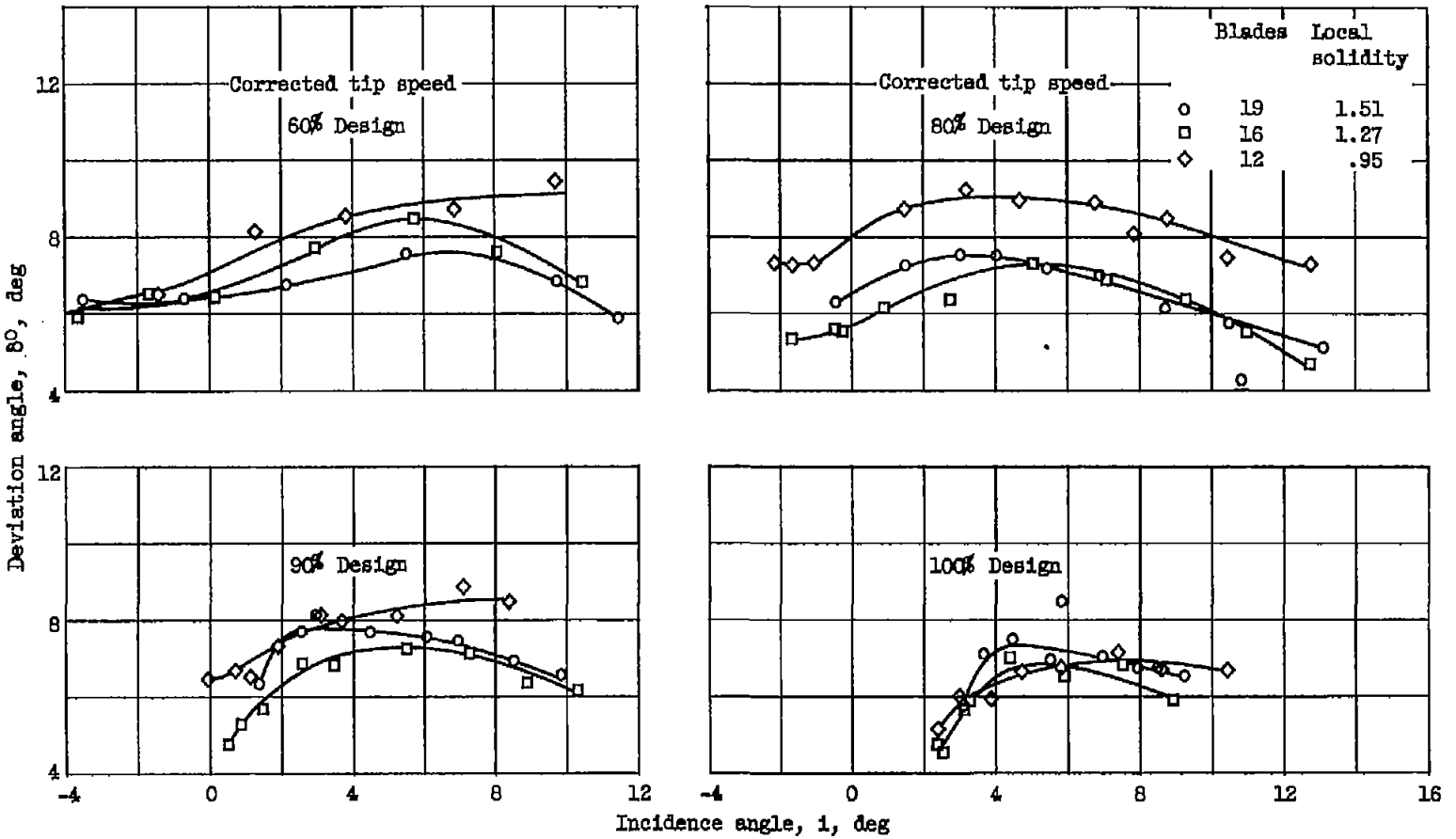

(a) Outlet radius (hub), 4.47 inches.

Figure 11. - Variation of deviation angle with incidence angle for three solidity levels.

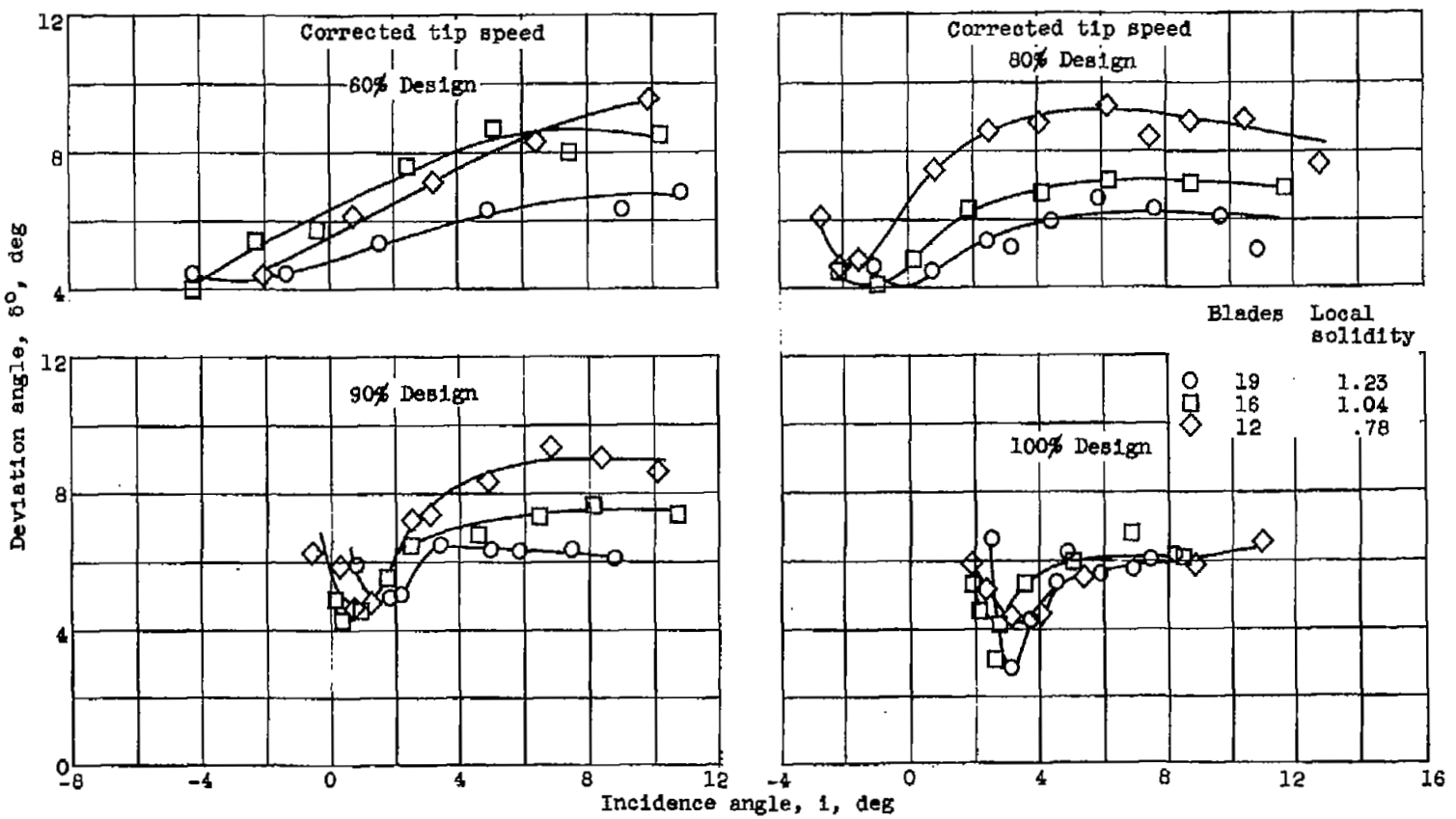

(b) Outlet radius (mean), 5.47 inches.

Figure 11. - Continued. Variation of deviation angle with incidence angle for three solidity levels.

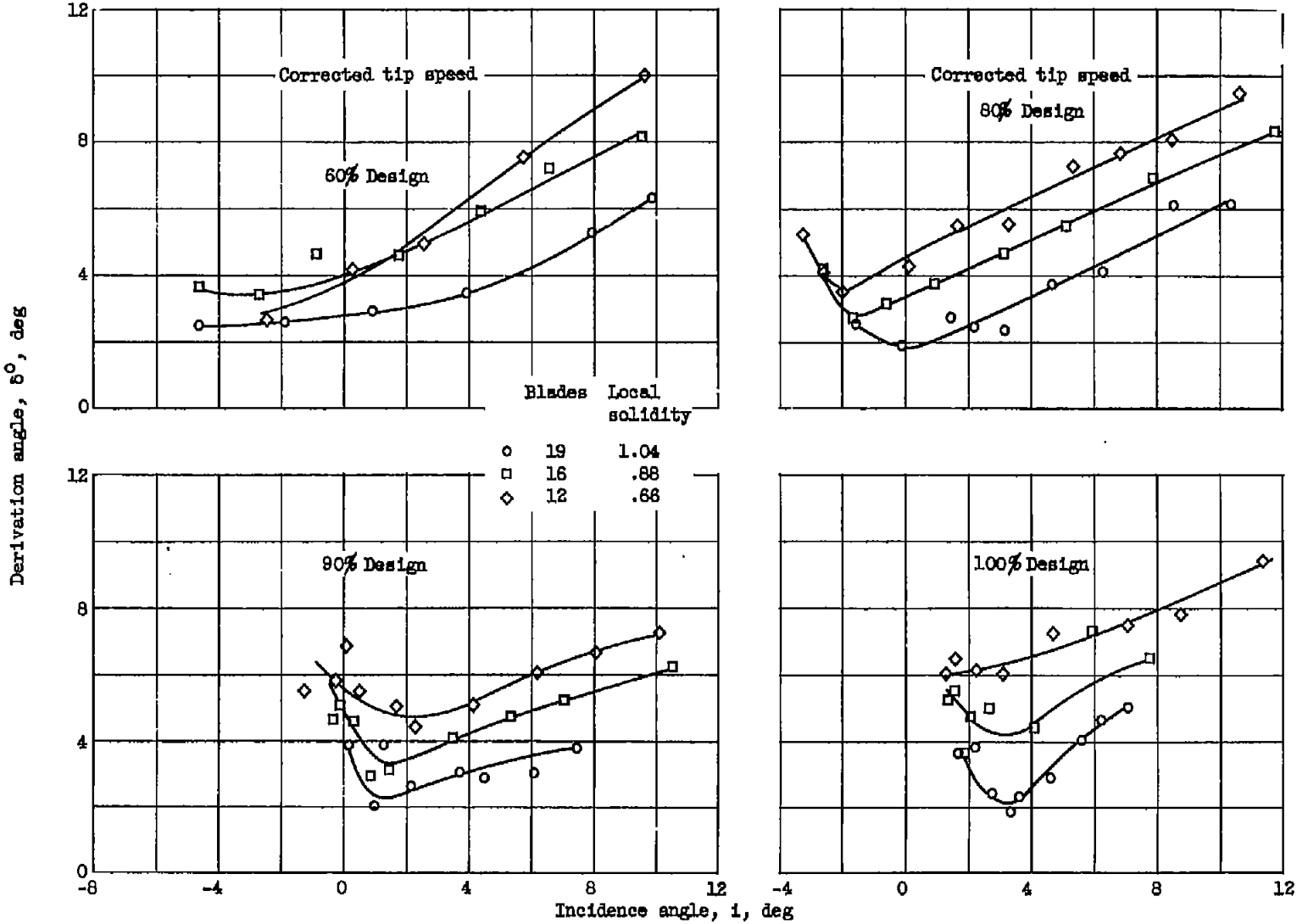

(c) Outlet radius (tip), 6.62 inches.

Figure 11. - Concluded. Variation of deviation angle with incidence angle for three solidity levels.

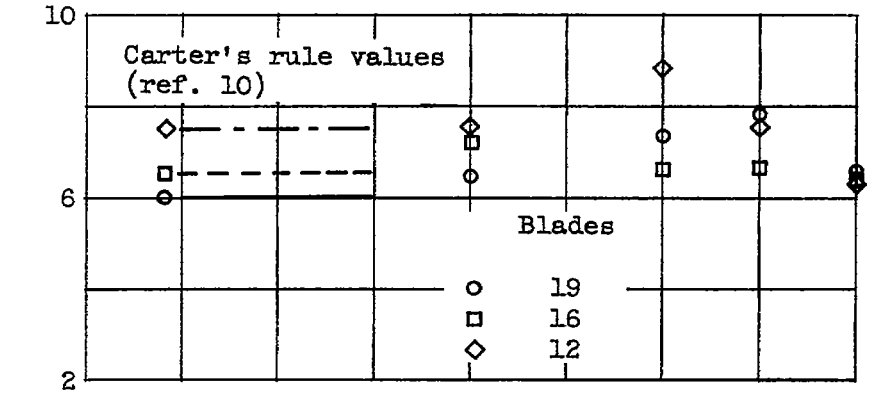

(a) Outlet radius (hub), 4.47 inches.

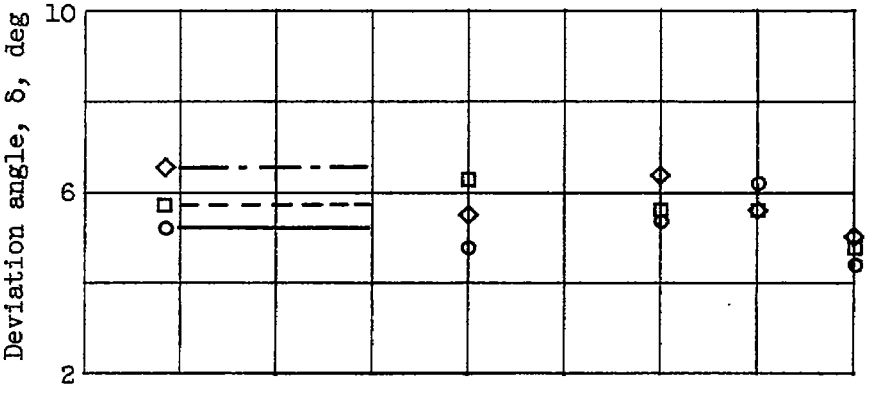

(b) Outlet radius (mean), 5.47 inches.

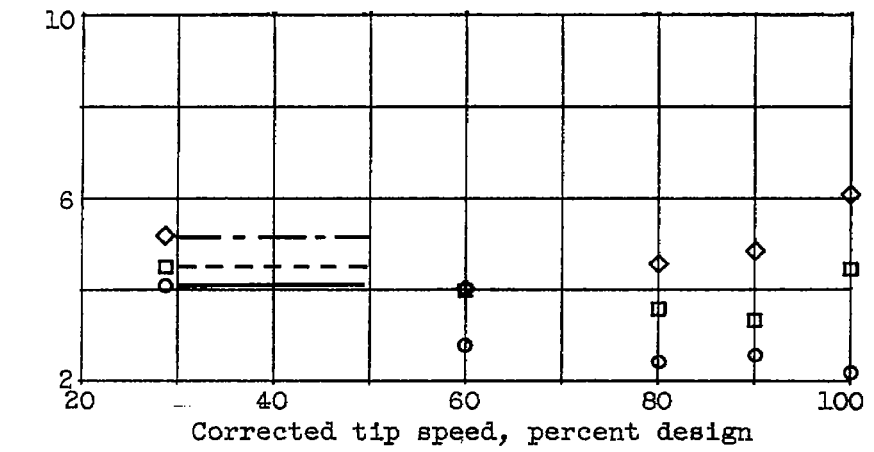

(c) Outlet radius (tip), 6.62 inches.

Figure 12. - Deviation angles at minimum-loss incidence angle for three solidity levels.

3530

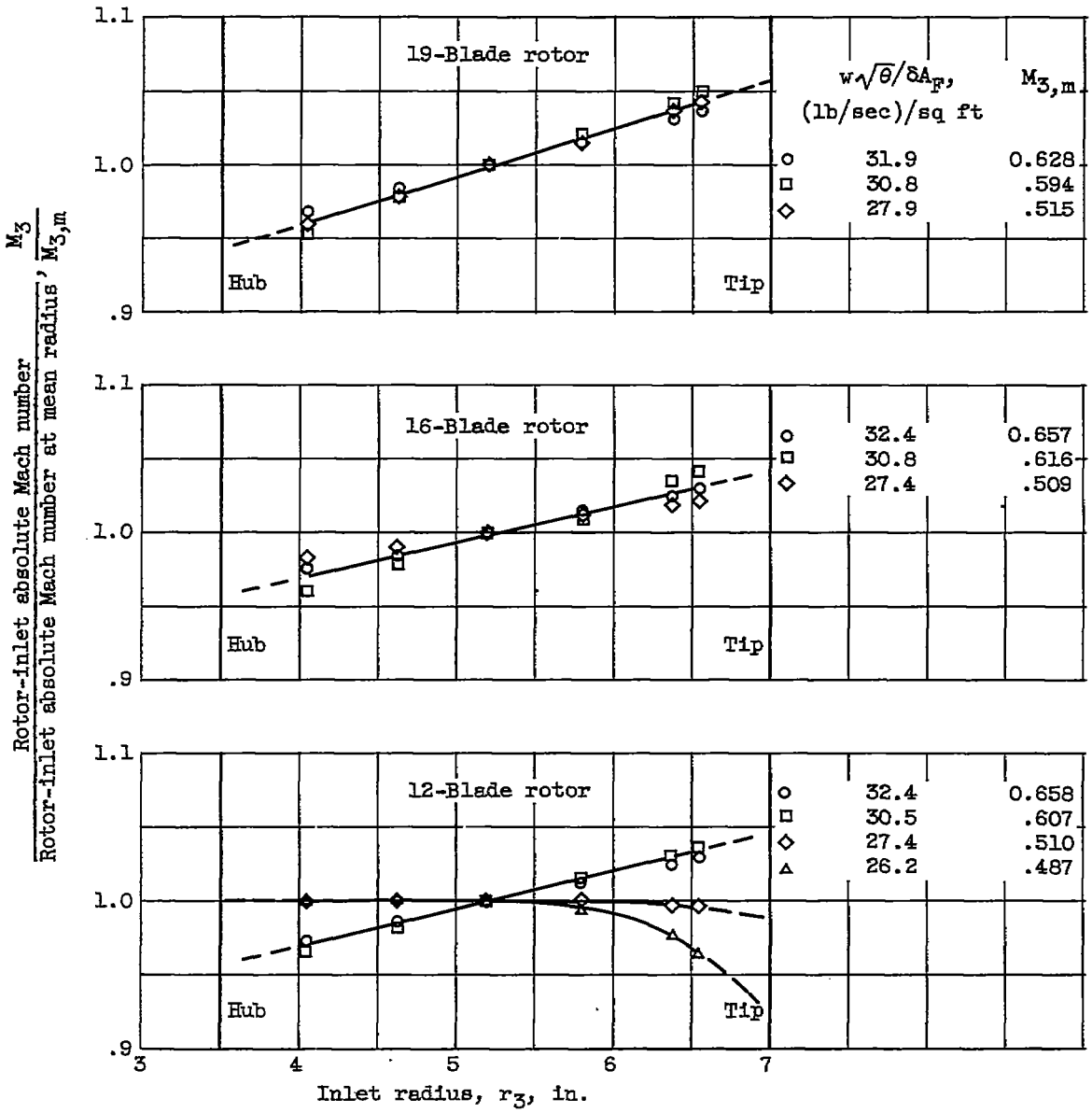

(a) Corrected tip speed, 100-percent design.

Figure 13. - Radial variation of rotor-inlet absolute Mach number.

[redacted]

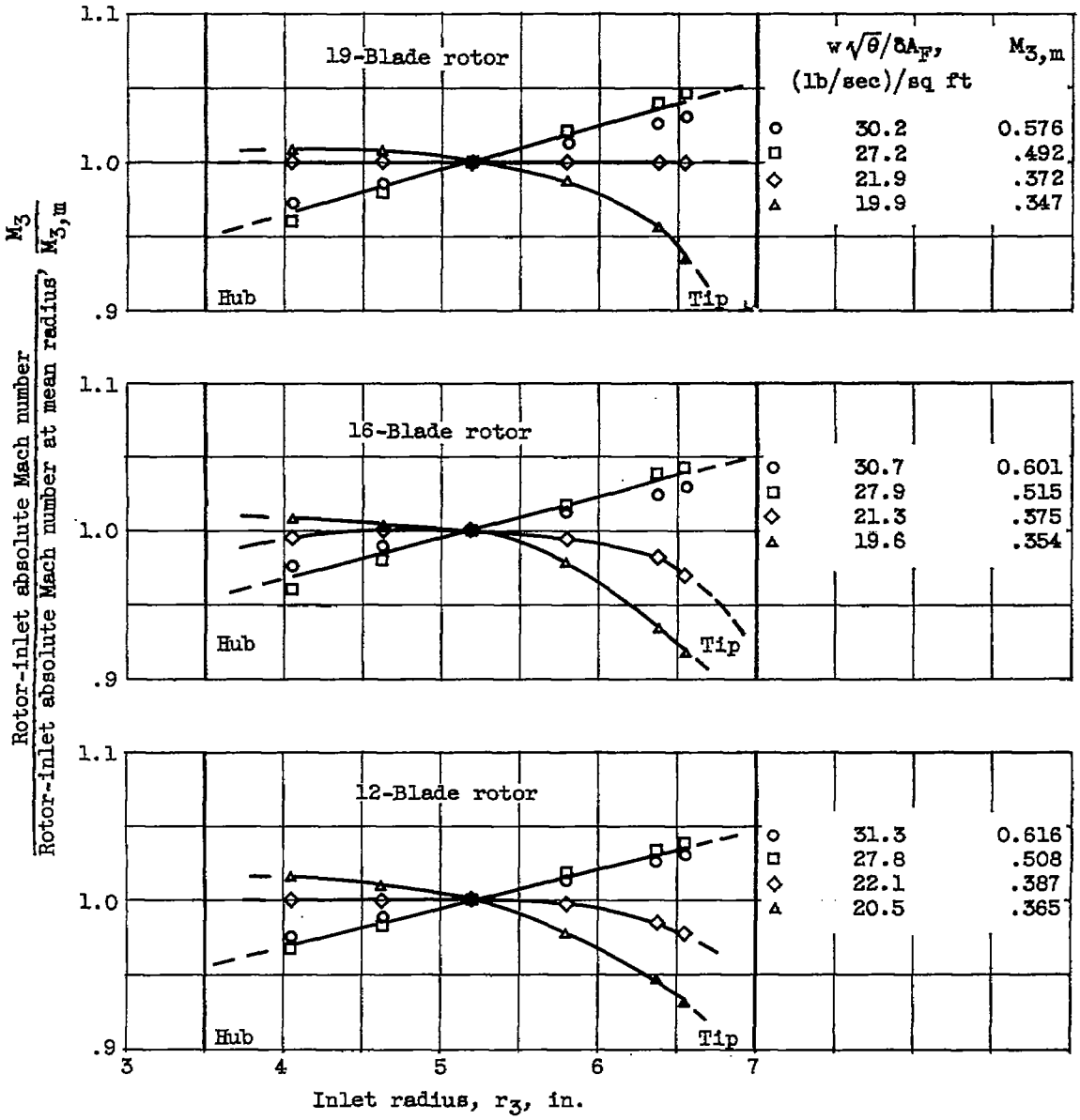

(b) Corrected tip speed, 80-percent design.

Figure 13. - Concluded. Radial variation of rotor-inlet absolute Mach number.

[redacted]

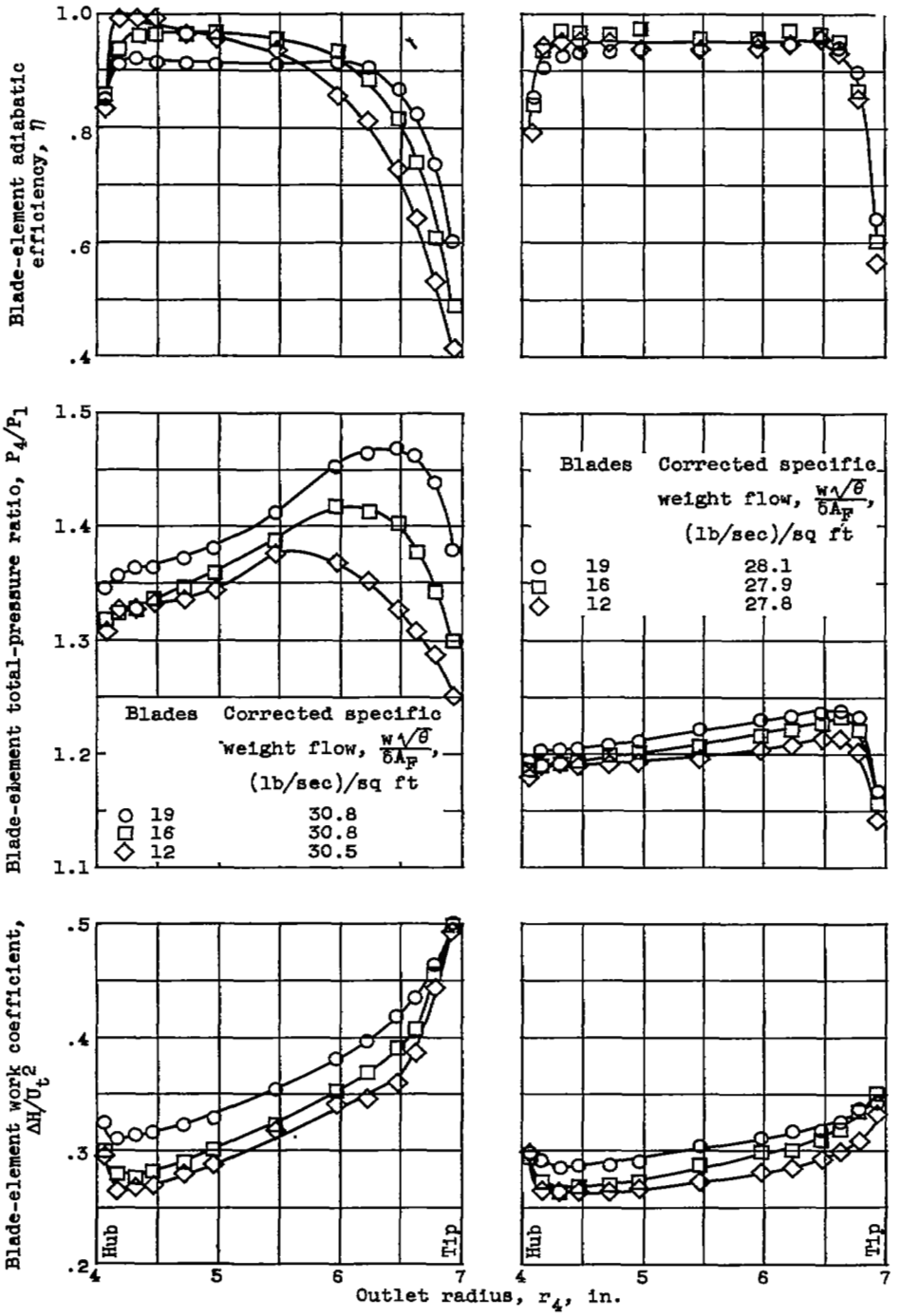

(a) Corrected tip speed, 100-percent design.

(b) Corrected tip speed, 80-percent design.

Figure 14. - Radial variation of blade-element adiabatic efficiency, total-pressure ratio, and work coefficient (nondimensional temperature rise) for three solidity levels.

[redacted]

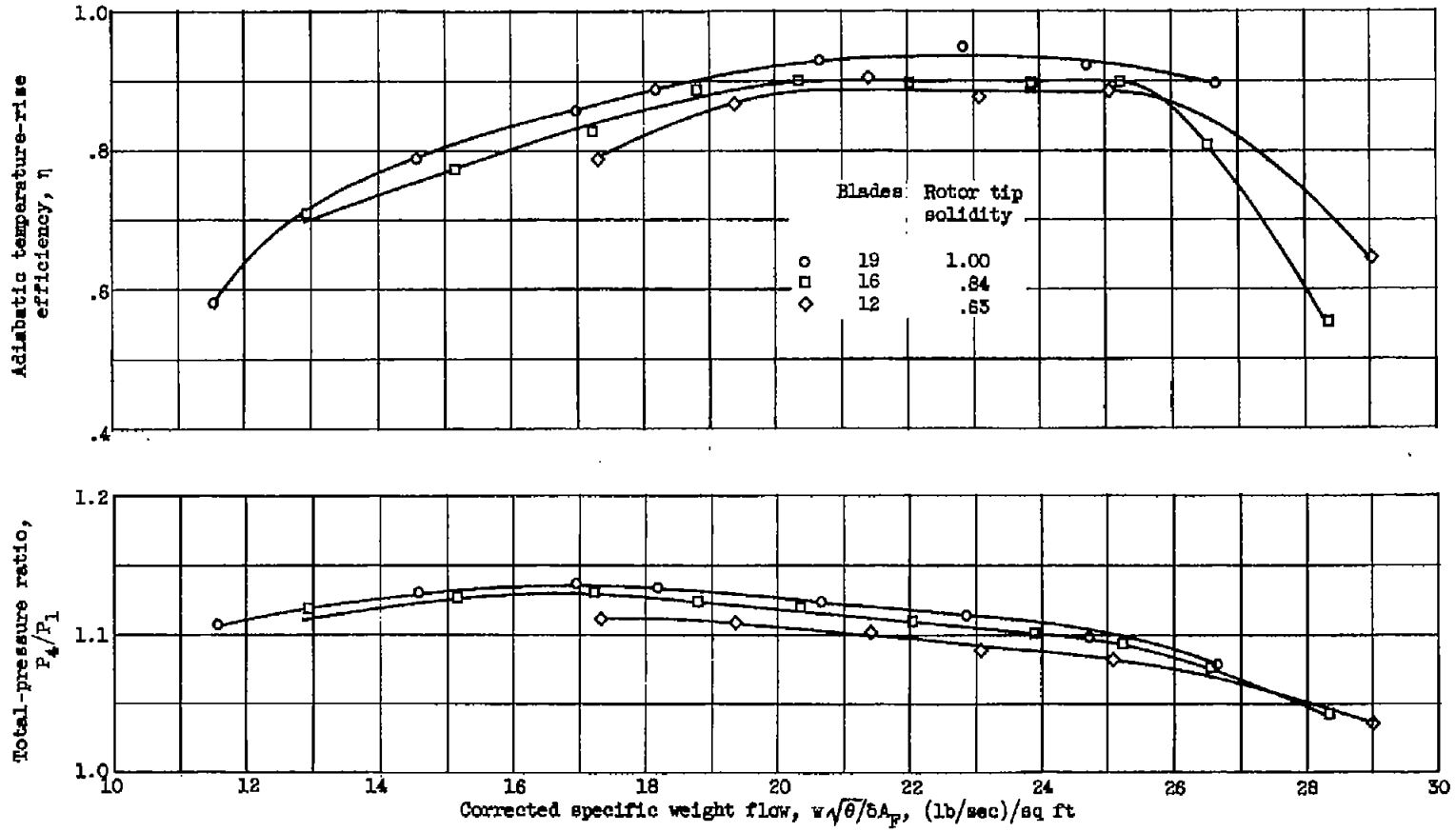

(a) Corrected tip speed, 60-percent design.

Figure 15. - Mass-averaged rotor performance for three solidity levels.

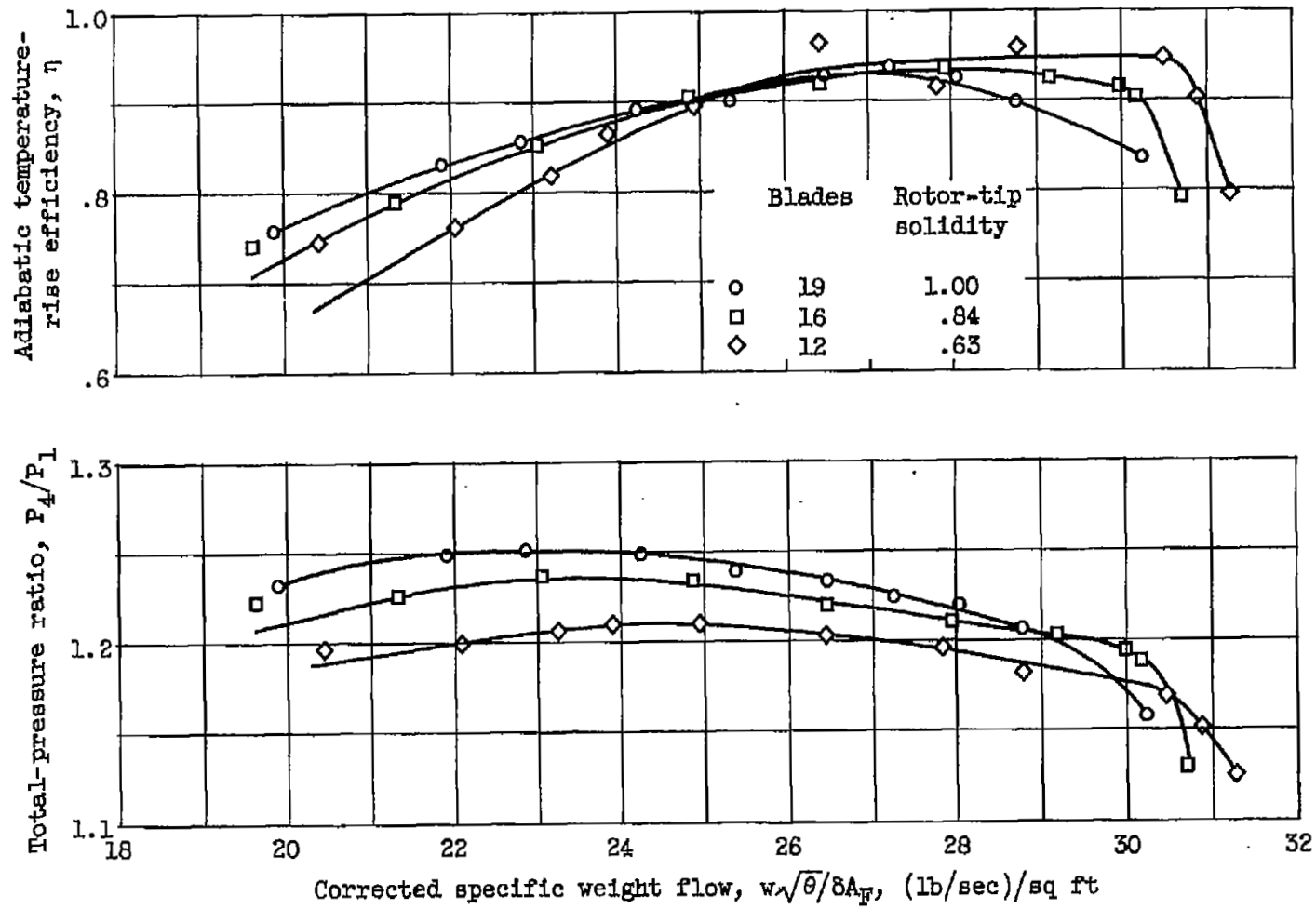

(b) Corrected tip speed, 80-percent design.

Figure 15. - Continued. Mass-averaged rotor performance for three solidity levels.

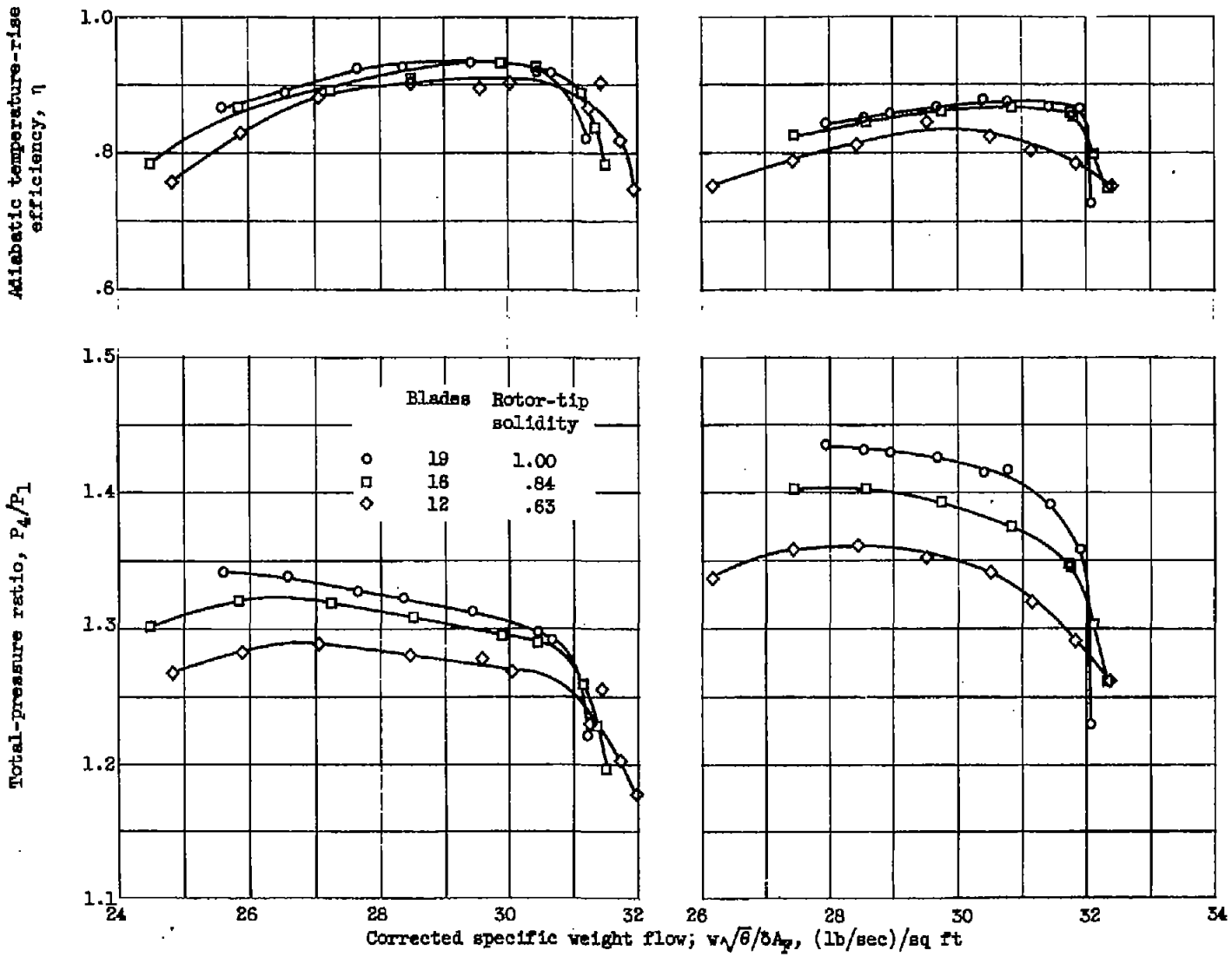

(c) Corrected tip speed, 90-percent design.

(d) Corrected tip speed, 100-percent design.

Figure 15. - Concluded. Mass averaged rotor performance for three solidity levels.